3 Experimental Results and Preliminary Discussion

3.1 Hot Compression Tests

The true stress-true strain curves were typical of materials undergoing softening by dynamic recovery and, when conditions were appropriate softening by DRX. As expected at higher strain rates the flow stress was higher. And when the testing temperature was lower the flow stress was also higher. The plots on fig. 3.1 through fig. 3.8 show the hot compression curves of Cu A. The hot compression curves for Cu B are shown on fig. 3.9 through fig. 3.16. And likewise fig. 3.17 through fig. 3.24 show the curves for Cu C. A comparison at 600ºC and 650ºC between the three coppers (fig. 3.25 and fig. 3.26) shows that the flow curves were representative of softening due to dynamic recovery when the strain rate was high. The difference between each copper laid on the magnitude of the observable stresses. Under the same conditions of strain rate and temperature the peak stress attained by copper C was always the highest, followed by copper B and then copper A with the lowest peak stress value.

The beginnings of dynamic recrystallization (noticeable softening after the peak stress) were first noticed on the hot flow curve of 600ºC and $0.003s^{-1}$ for copper B (see fig. 3.25). Both coppers B and C seemed to recrystallize dynamically at the next slowest strain rate of $0.001s^{-1}$. When the temperature was raised 50ºC to 650ºC (see fig. 3.26) a peak stress that signaled DRX was meekly noticed at a strain rate of $0.03s^{-1}$ and for Cu B and Cu C only. At a slower strain rate of $0.003s^{-1}$ DRX was clearly present on the three coppers. As on lower temperatures at 700ºC in fig. 3.27 an incomplete dynamic recrystallization (absence of a clear steady state stress) was noticed on most of the hot flow curves for the three coppers. Only at the slowest strain rates and at 700ºC complete recrystallization was apparent, but micrograph analysis showed that homogeneous grain refinement was only reached for some of these strain rates ($0.01s^{-1}$ for Cu A, $0.003s^{-1}$ for Cu B and $0.001s^{-1}$ for both Cu B and C). The tests conducted at 750ºC (seen on fig. 3.28) showed single peak dynamic recrystallization of the strain rates considered except at $0.3s^{-1}$ for Cu C.

Subsequent peak stresses after the maximum stress peak (cyclic or multiple peak dynamic recrystallization) were noticed at the slowest strain rates of the 800ºC hot flow curves (seen on fig. 3.29). Multiple peak dynamic recrystallization was a general observation on most of the tests carried out at 850ºC, 900ºC and, 950ºC for the three coppers (see figures 3.30, 3.31 and 3.32). Only at the highest strain rates ($0.3s^{-1}$, $0.1s^{-1}$) of these latter temperatures, dynamic recrystallization was of the single peak type. As a general feature and similar to the dynamic recovery case, the largest stresses observed under dynamic recrystallization conditions corresponded to copper C, followed by copper B and then Cu A.

The oxygen content correlates well with the observed increase of flow stress among the three coppers. Copper A has 26ppm of O, copper B has 46ppm and copper C has 62ppm. No other residual element on the three 99.9% pure coppers follows the same increasing order. Phosphorus, which is used to de-oxidize molten copper, follows an inverse order, being in highest quantity in Cu A and lowest in Cu C. The correlation between the oxygen content and a higher flow stress initially suggests that oxygen is responsible either by solid solution strengthening or by precipitation of oxides. The strengthening influence of oxygen in copper had been known some time [1]. Several authors have suggested that solute oxygen atoms effectively interact with dislocations to raise the flow stress [2, 3]. Other authors [4, 5] have theorized that interstitial oxygen atoms at temperatures below 700ºC create nonsymmetrical stress fields, which

effectively interact with both edge and screw dislocations. However the dislocation-oxygen atom interaction study was not presented. On the other hand the Cu-O phase diagram does predict the presence of copper oxides. The formation of precipitates at lower temperatures was considered as the reason for the observed hot flow behavior. In the case of the fire-refined coppers used on this work the residual content also had to be considered. If precipitation strengthening was occurring then precipitates had to be characterized. Either through one mechanism or another the oxygen content appeared to be mainly responsible of the different results seen after the hot compression tests of Cu A, Cu B and Cu C.

Other factors that could have produced the observed difference are the initial grain size, a strong texture difference or possibly the inclusions present in the coppers. However none of the latter arguments could be proven to be of having been of influence. First the initial grain size is known to affect flow stress however after DRX the grain size influence disappears. And in the coppers of this study the flow stress difference remained. Also the three coppers had large initial grain sizes, which considering the logarithmic grain size relationships (to be explained later) the three coppers were equally affected. The initial grain sizes for Cu A, Cu B and Cu C were 637µm, 570µm and 530µm. The initial texture was not examined but the assumption is made that the three coppers possess a comparable and weak texture components, because the microstructure is the result of hot forming where DRX occurs, which leaves relatively weak texture components. The influence of the inclusions required a study, whose results will be presented later.

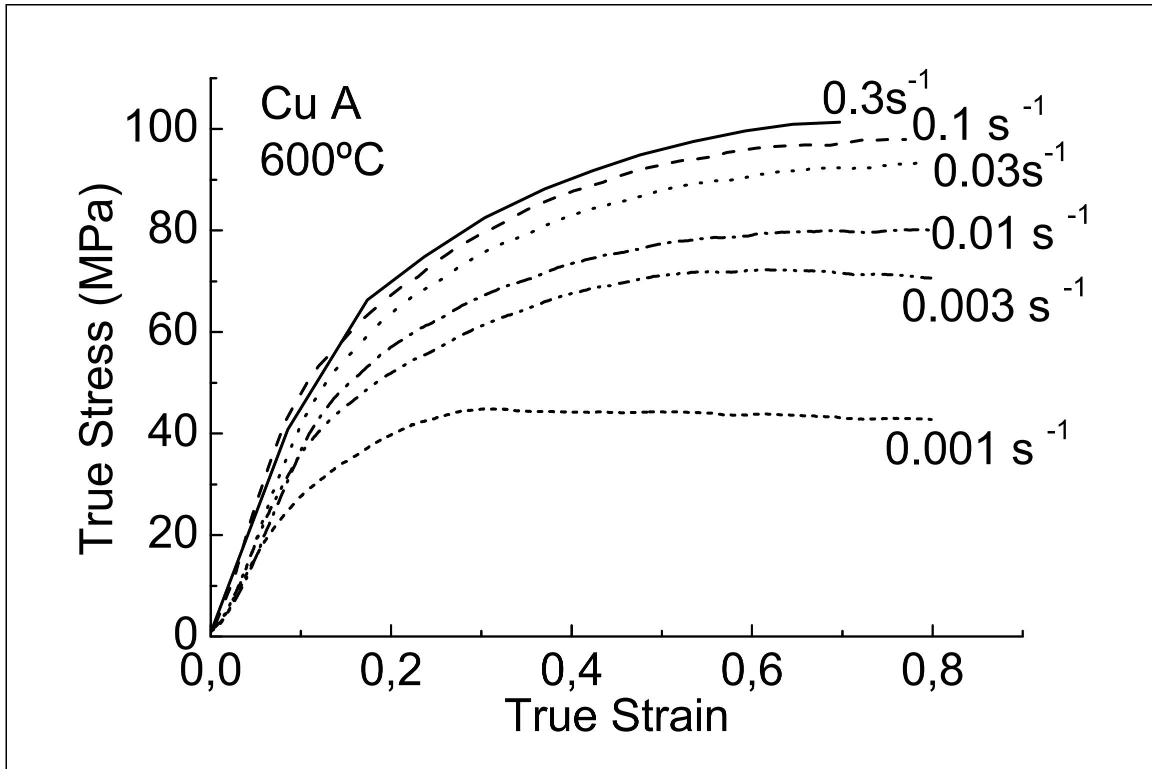

Fig. 3.1 Hot compression curves of Cu A at 600ºC and different strain rates.

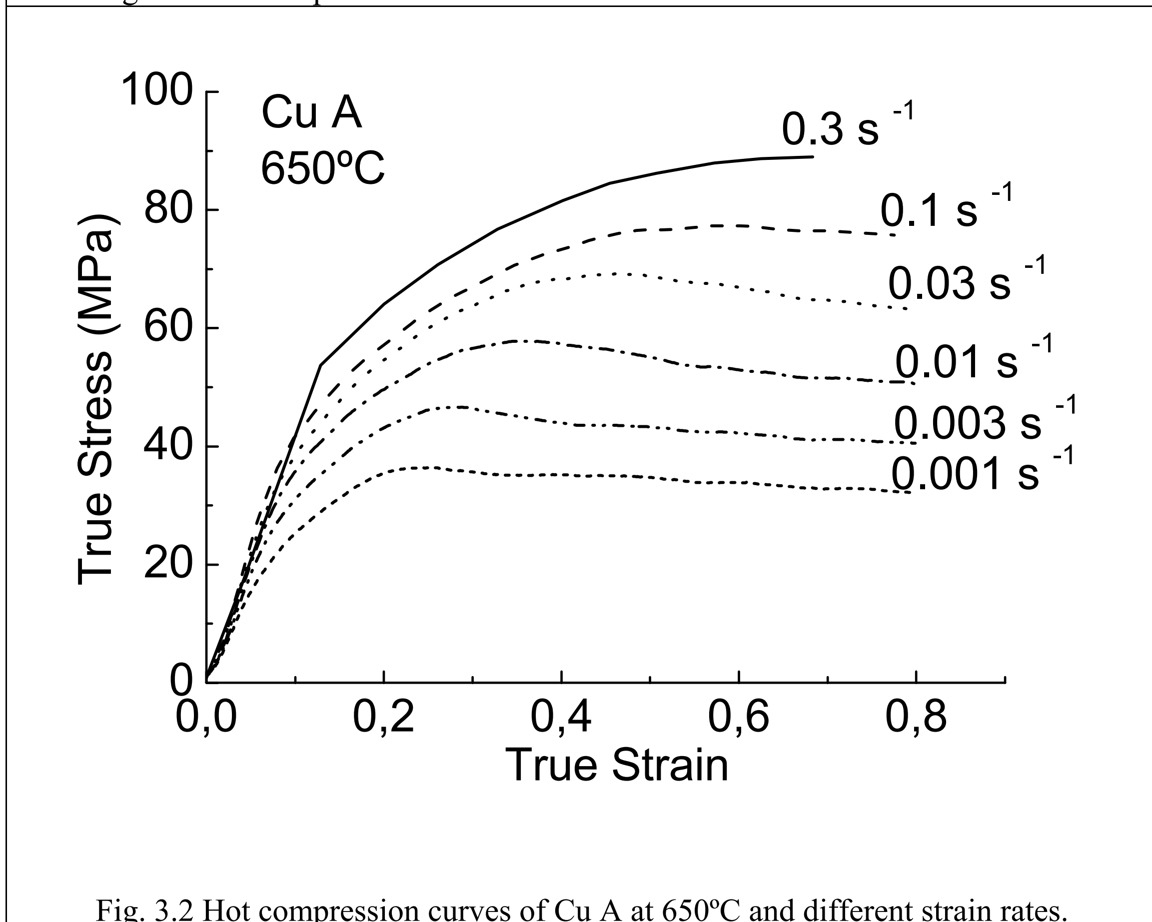

Fig. 3.2 Hot compression curves of Cu A at 650ºC and different strain rates.

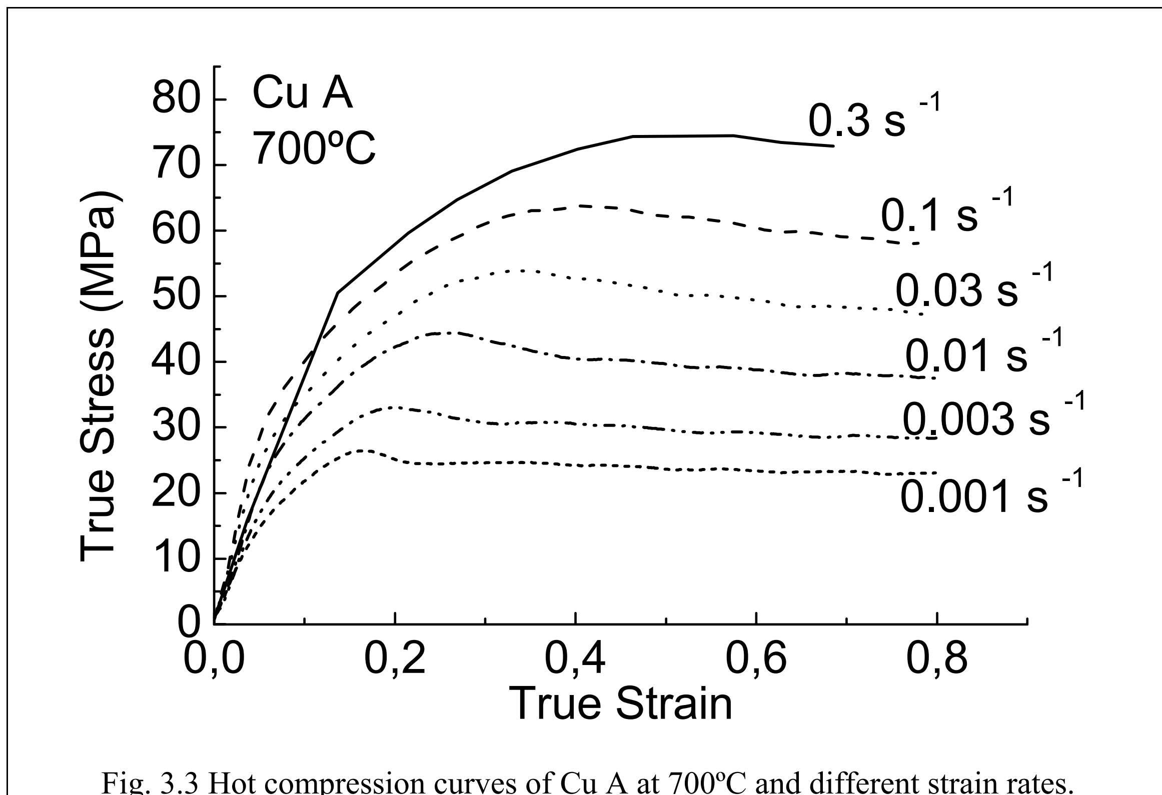

Fig. 3.3 Hot compression curves of Cu A at 700ºC and different strain rates.

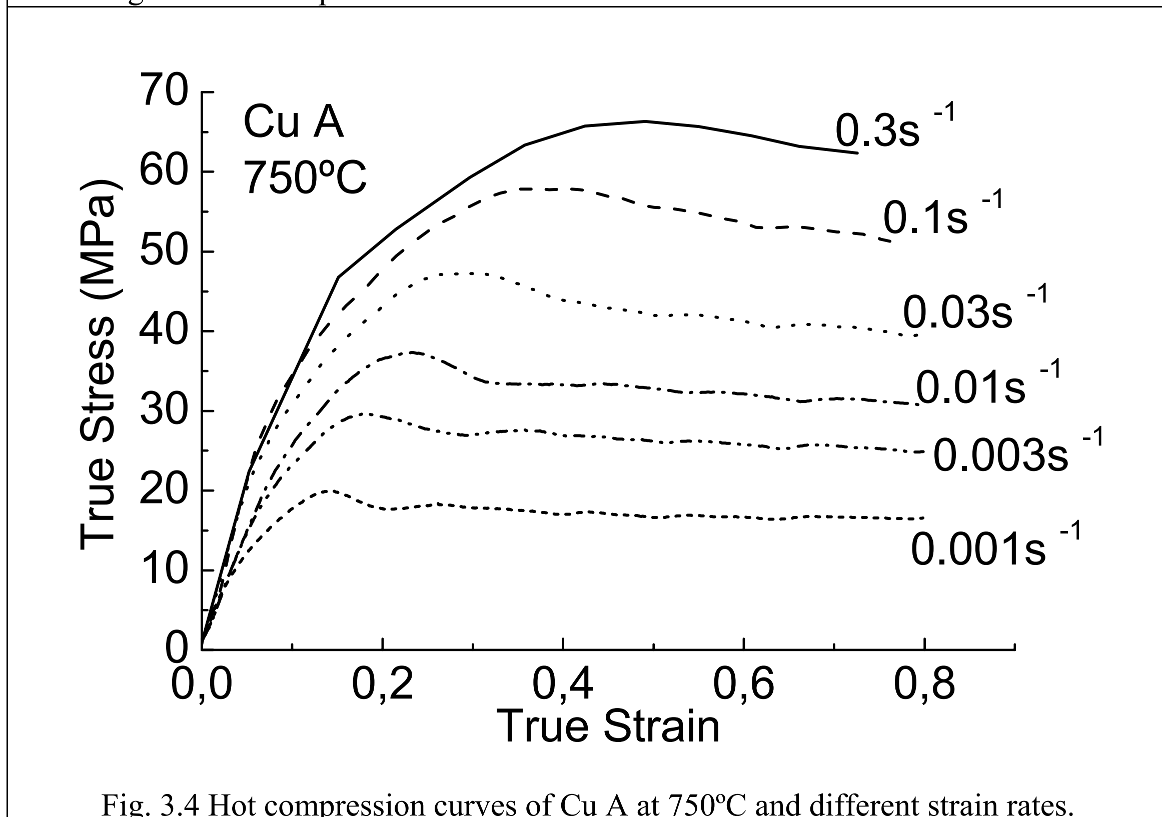

Fig. 3.4 Hot compression curves of Cu A at 750ºC and different strain rates.

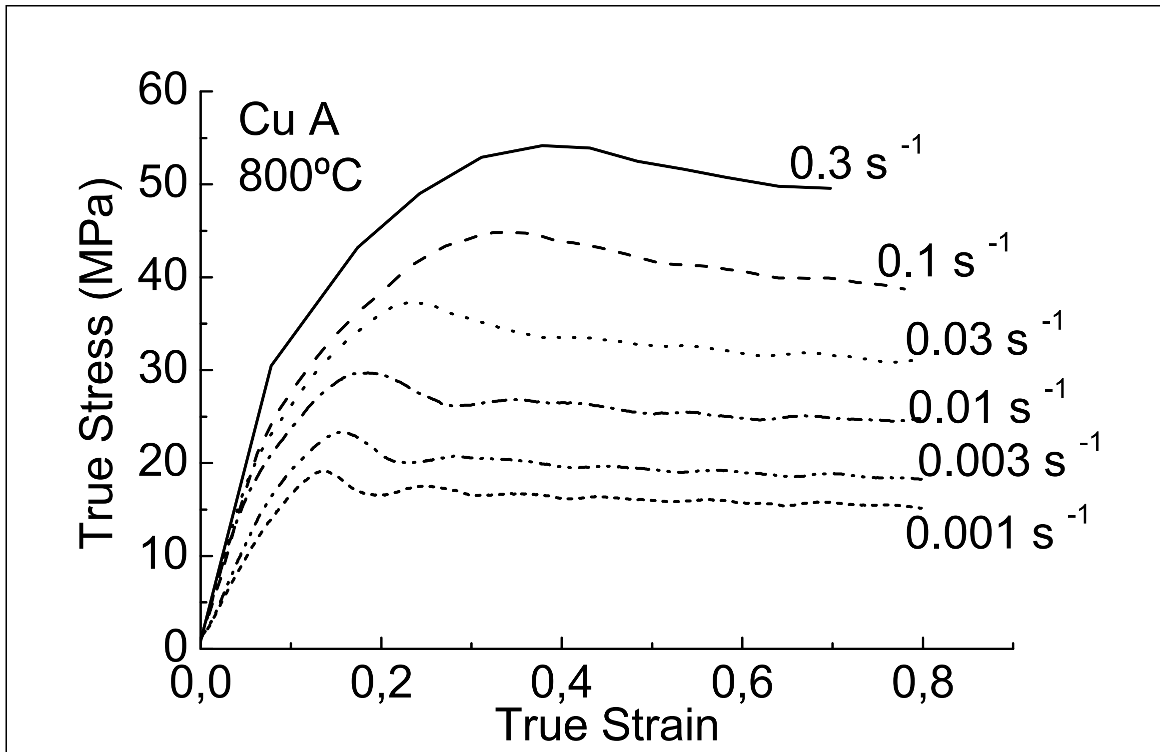

Fig. 3.5 Hot compression curves of Cu A at 800ºC and different strain rates.

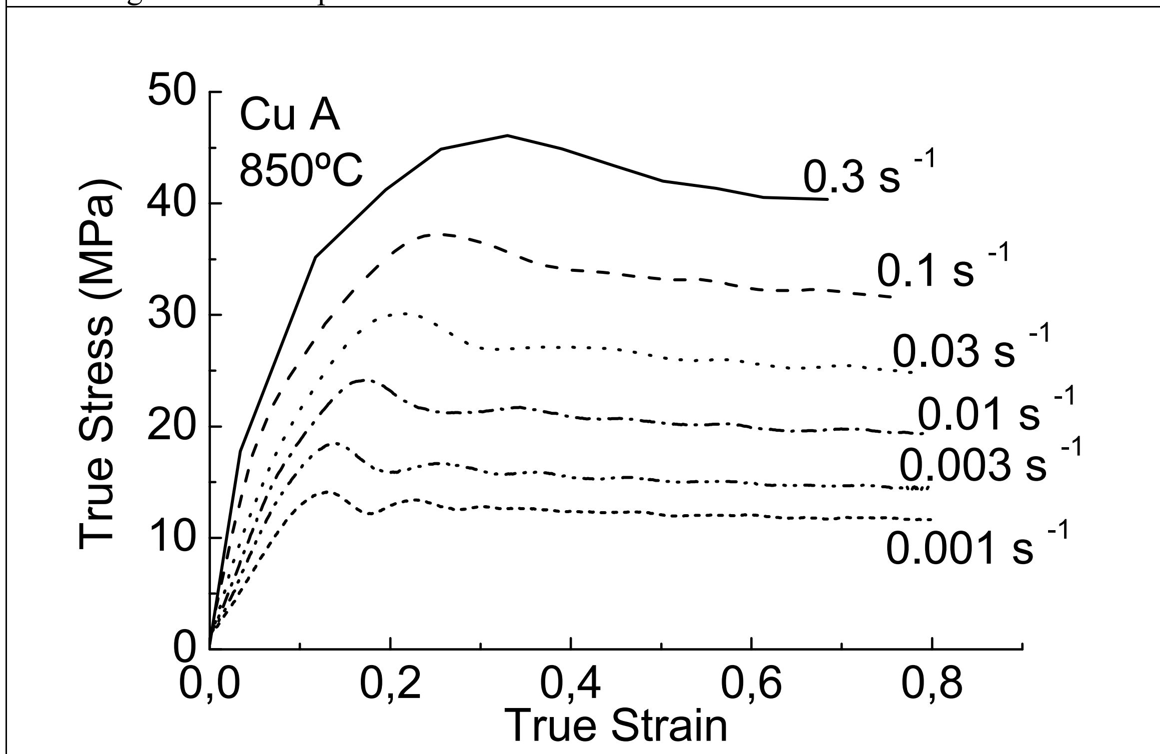

Fig. 3.6 Hot compression curves of Cu A at 850ºC and different strain rates.

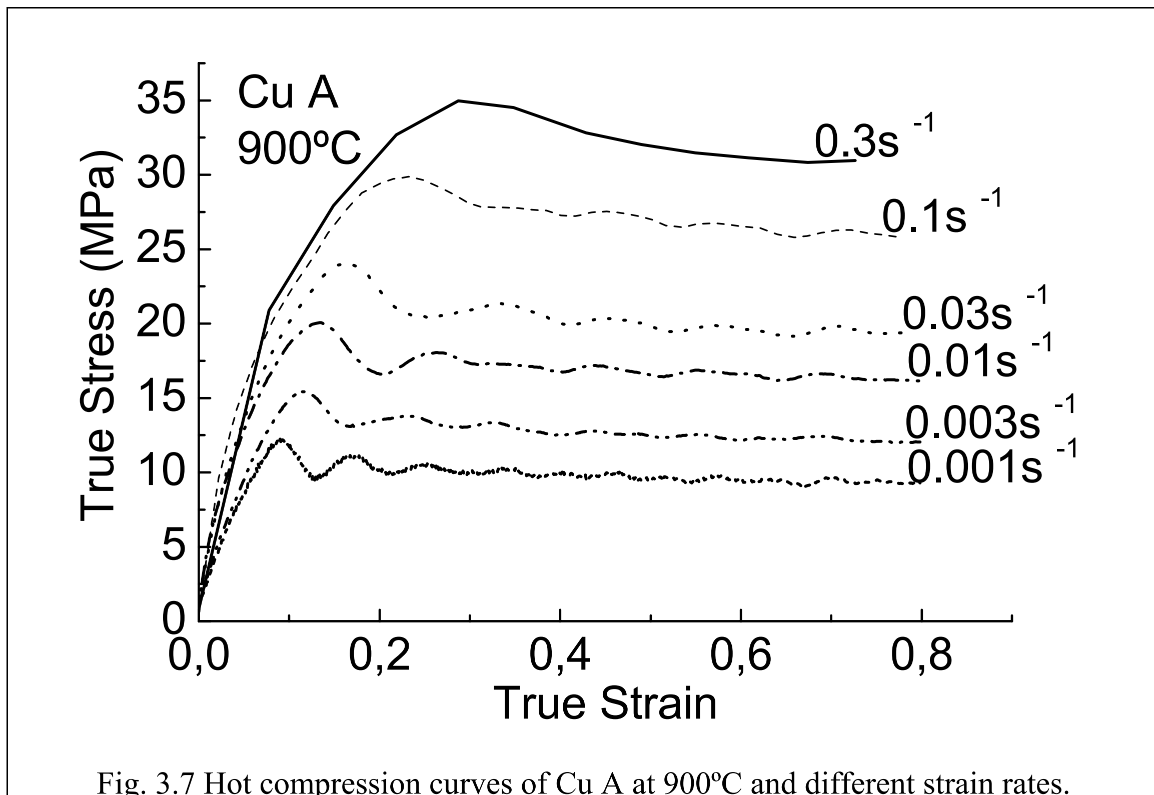

Fig. 3.7 Hot compression curves of Cu A at 900ºC and different strain rates.

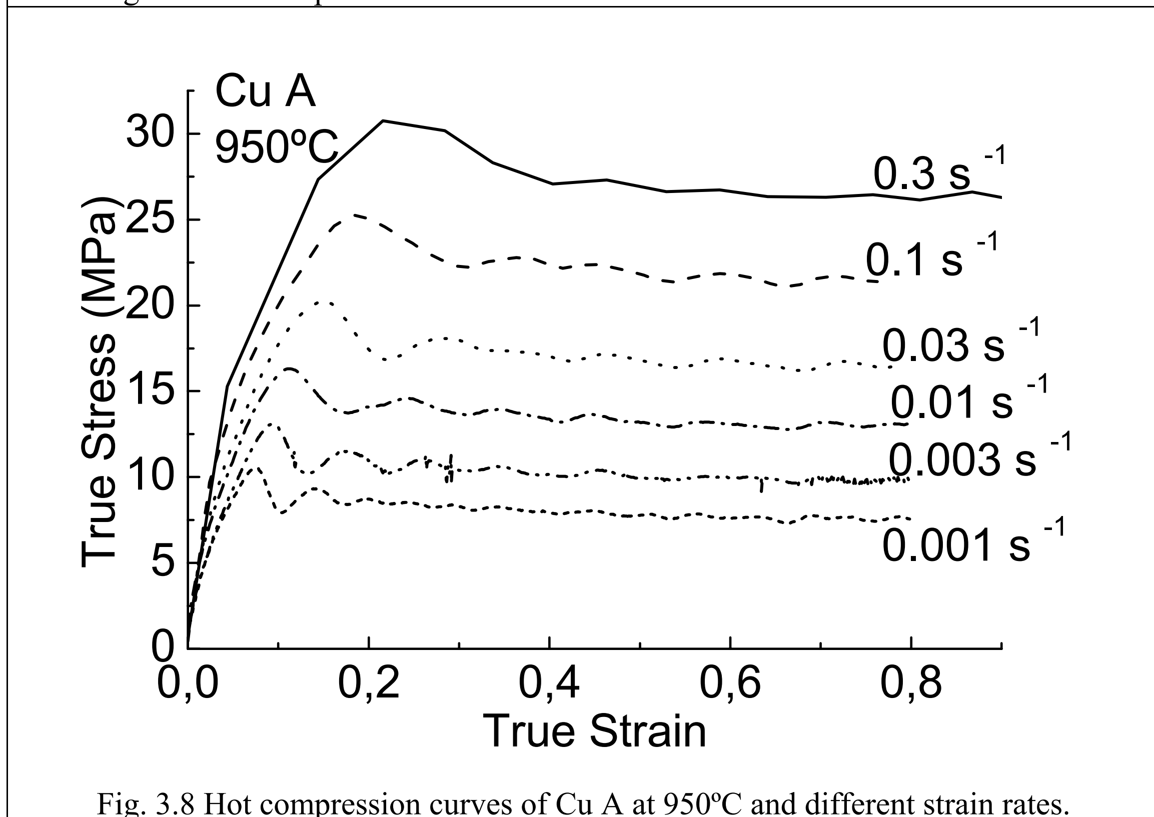

Fig. 3.8 Hot compression curves of Cu A at 950ºC and different strain rates.

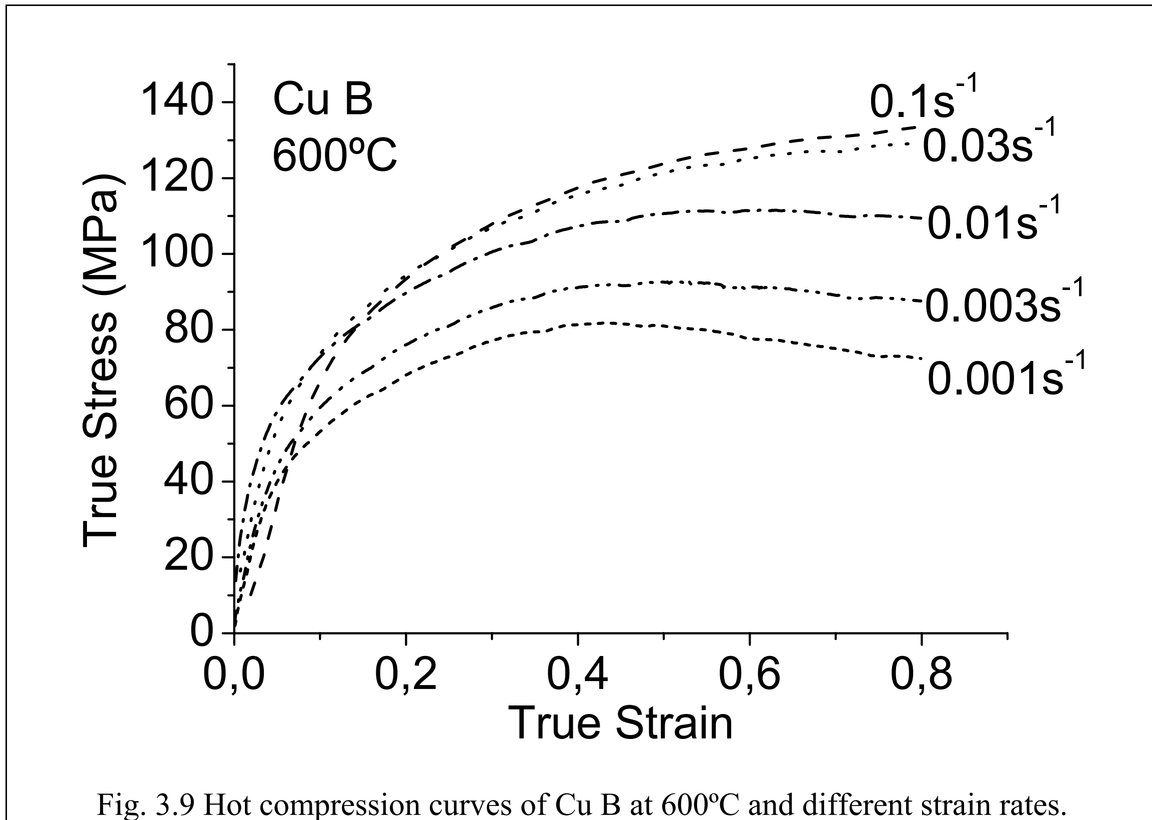

Fig. 3.9 Hot compression curves of Cu B at 600ºC and different strain rates.

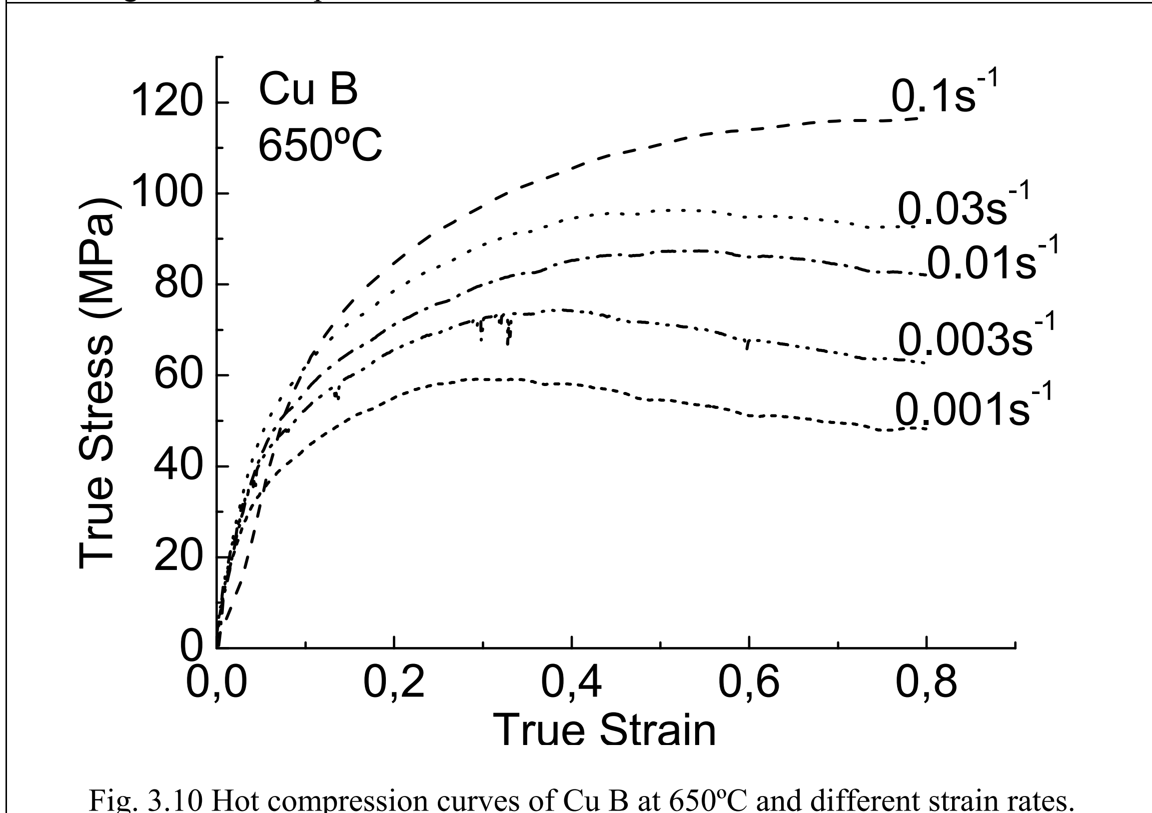

Fig. 3.10 Hot compression curves of Cu B at 650ºC and different strain rates.

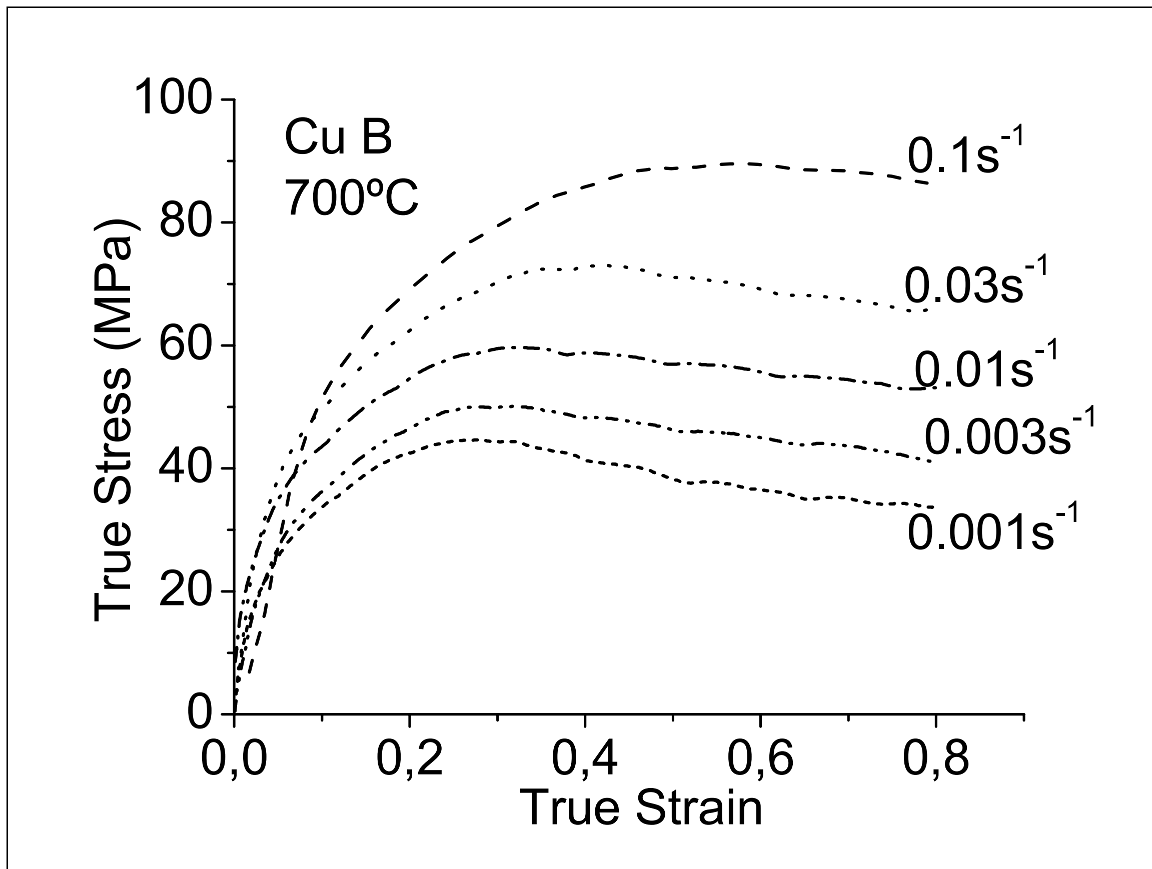

Fig. 3.11 Hot compression curves of Cu B at 700ºC and different strain rates.

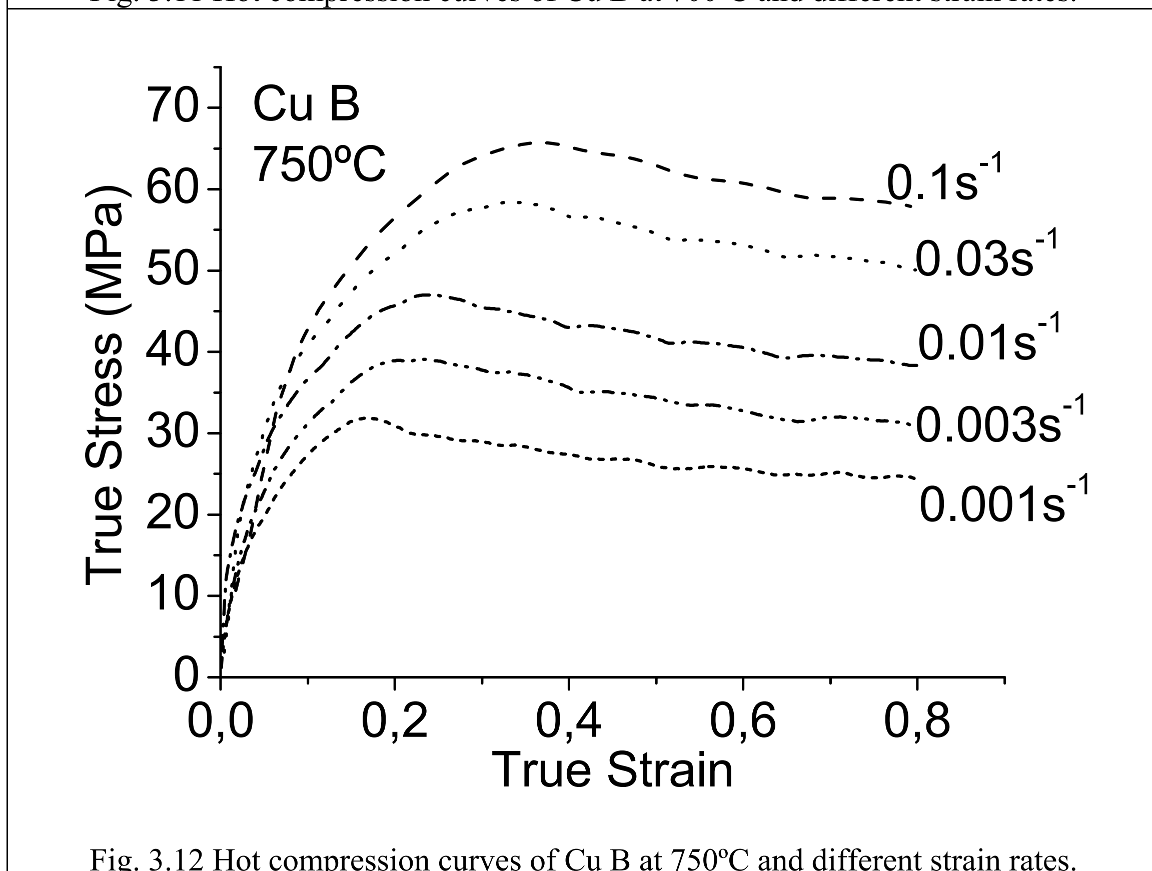

Fig. 3.12 Hot compression curves of Cu B at 750ºC and different strain rates.

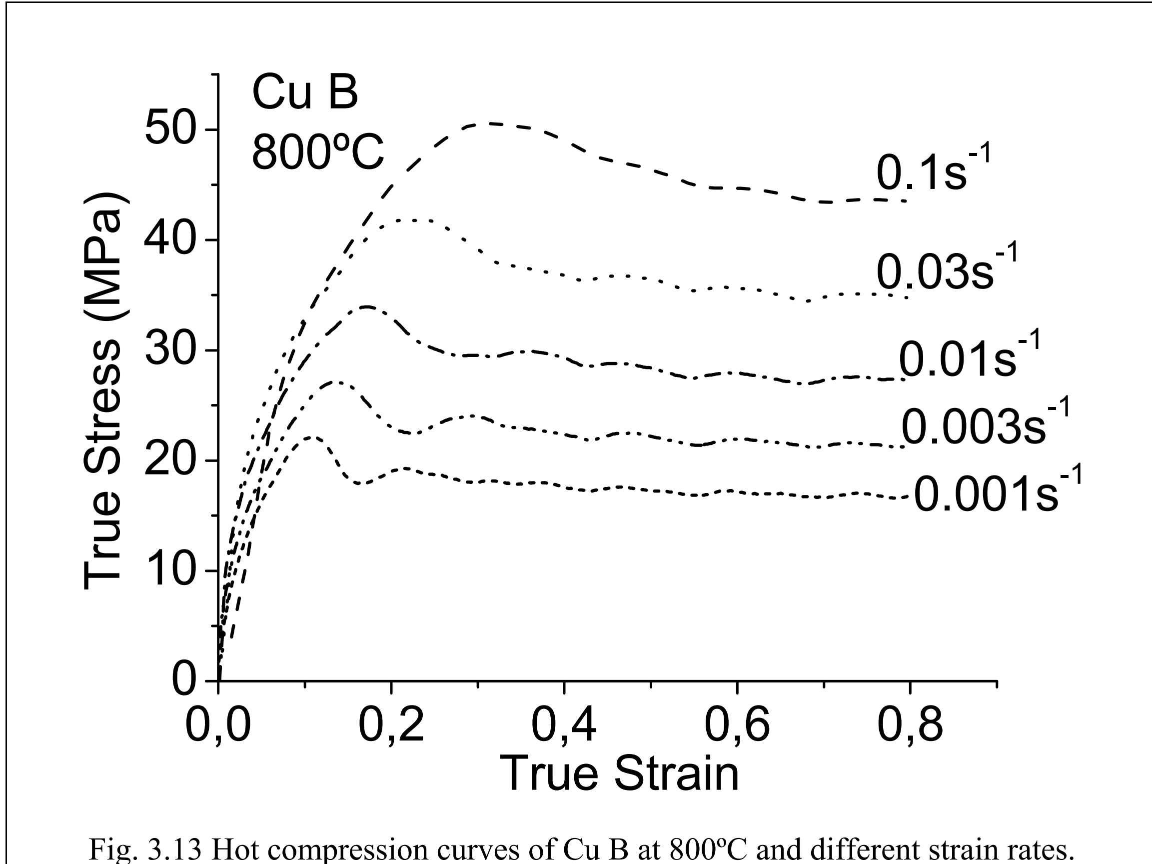

Fig. 3.13 Hot compression curves of Cu B at 800ºC and different strain rates.

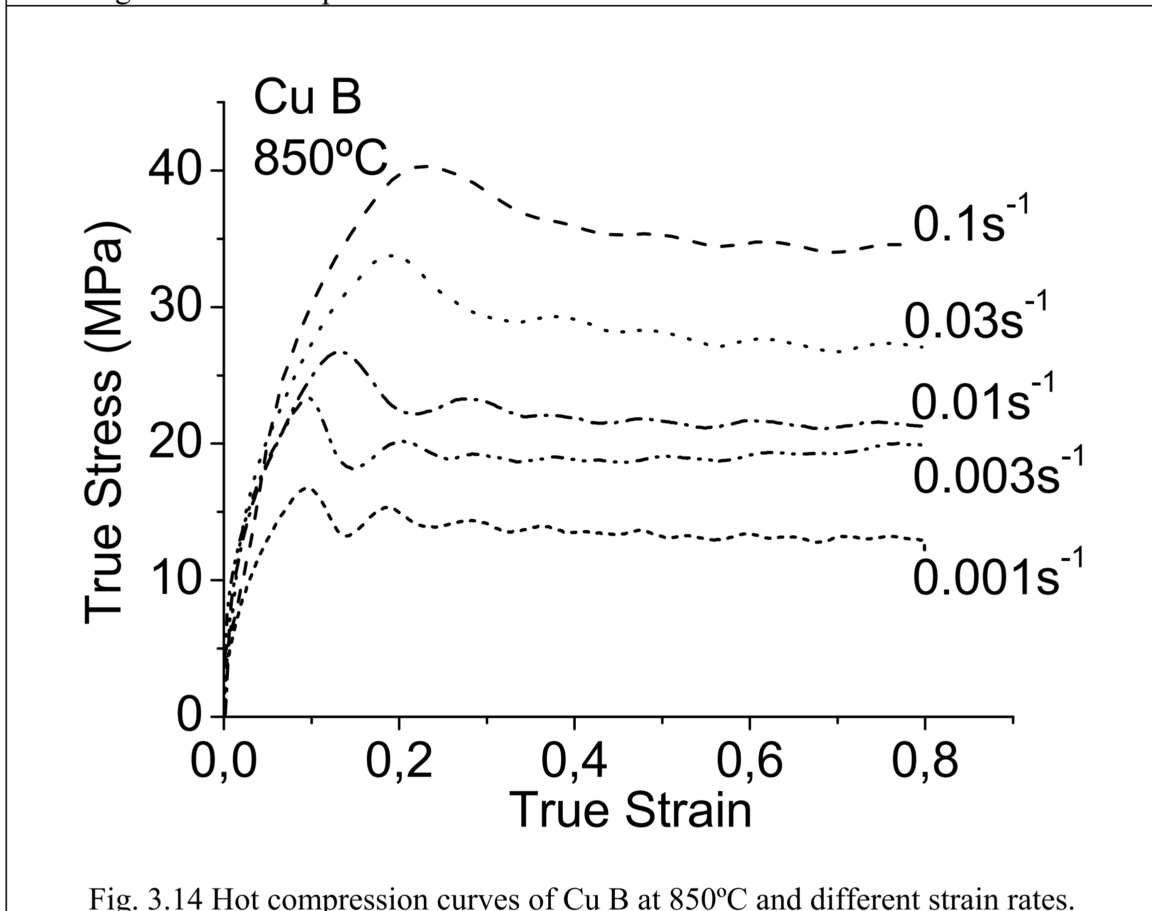

Fig. 3.14 Hot compression curves of Cu B at 850ºC and different strain rates.

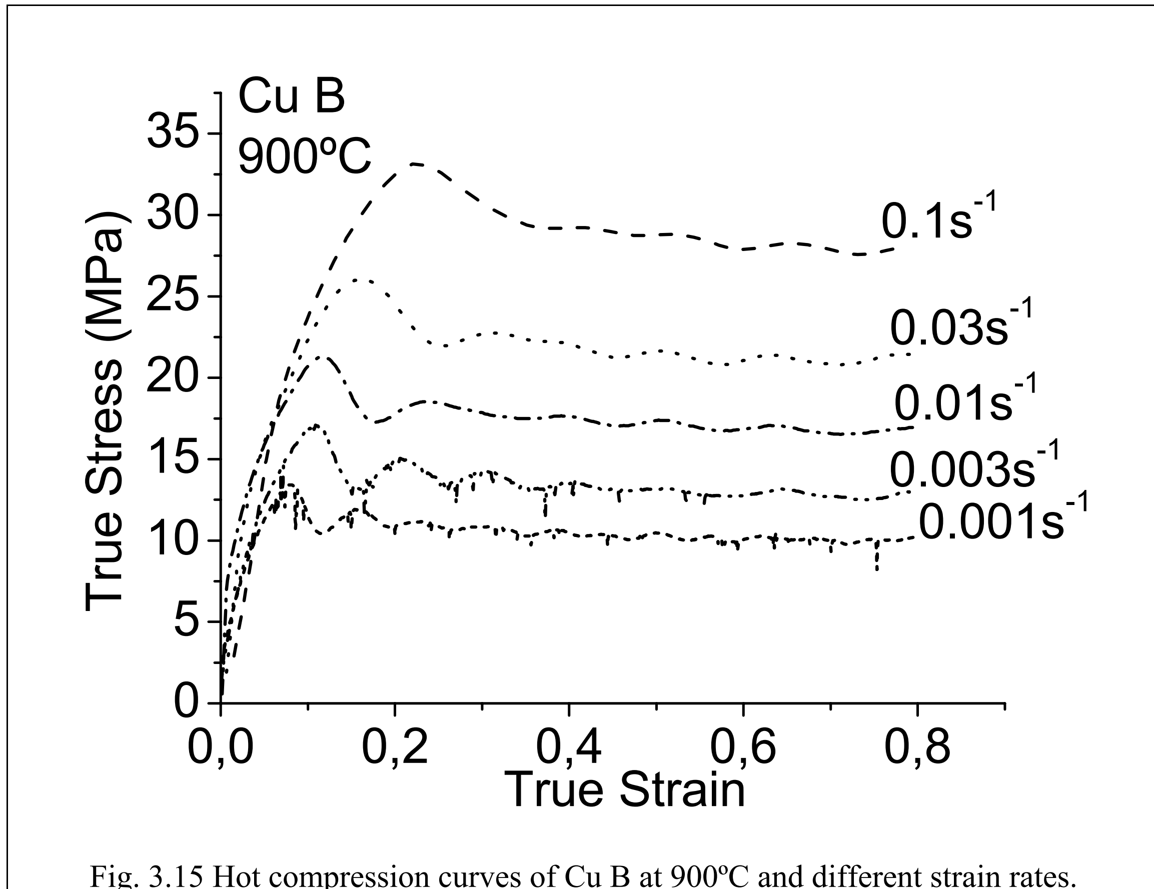

Fig. 3.15 Hot compression curves of Cu B at 900ºC and different strain rates.

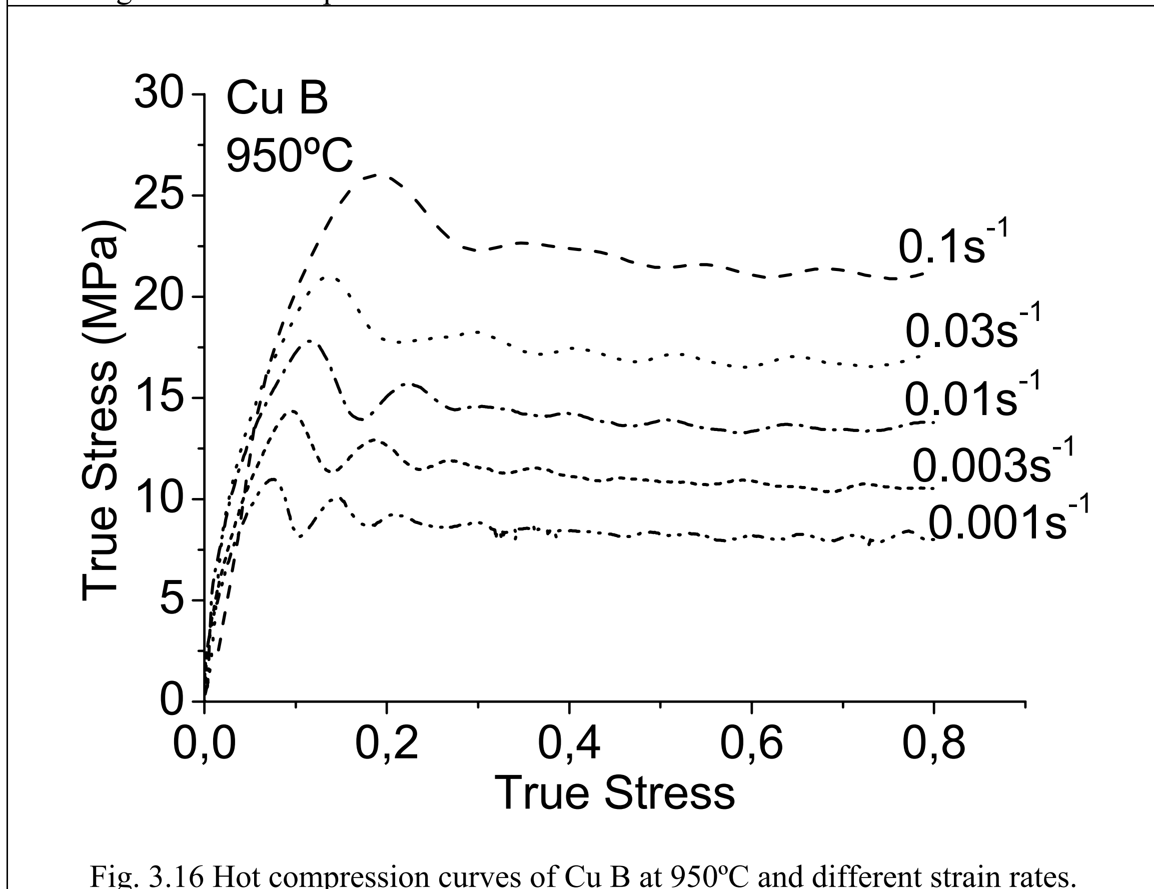

Fig. 3.16 Hot compression curves of Cu B at 950ºC and different strain rates.

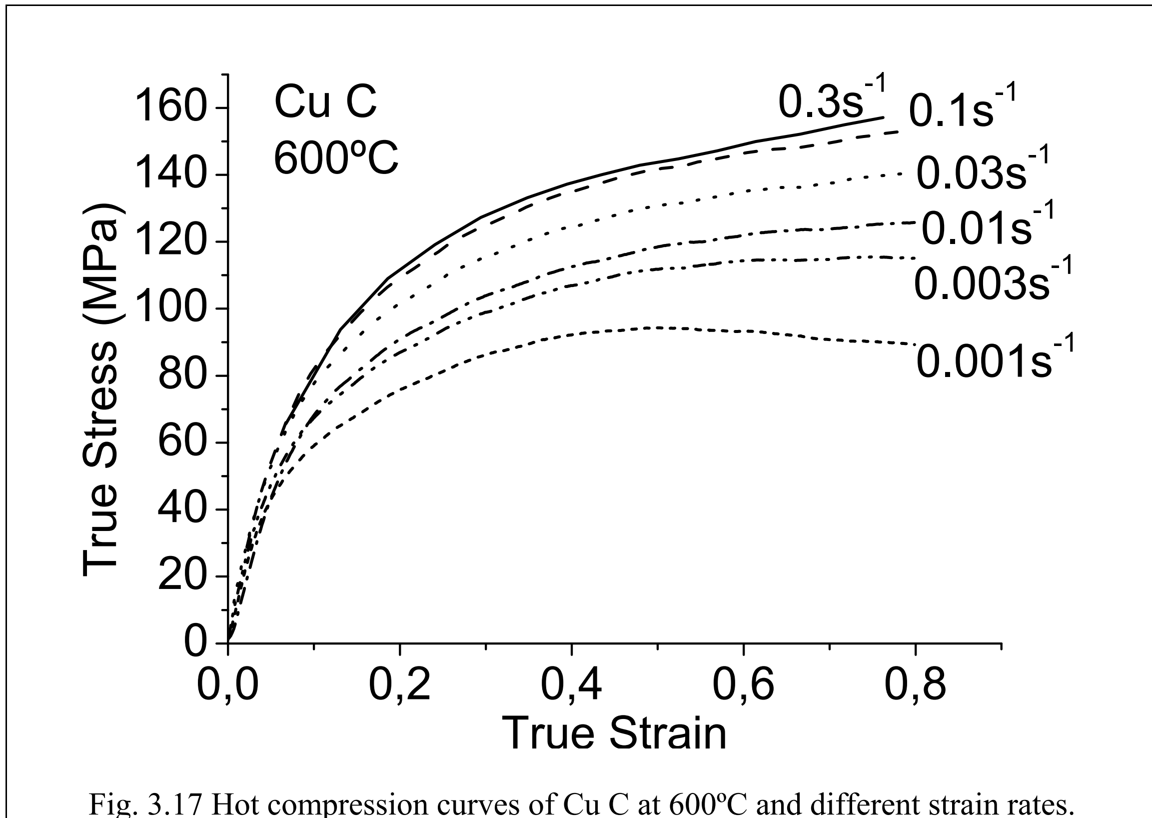

Fig. 3.17 Hot compression curves of Cu C at 600ºC and different strain rates.

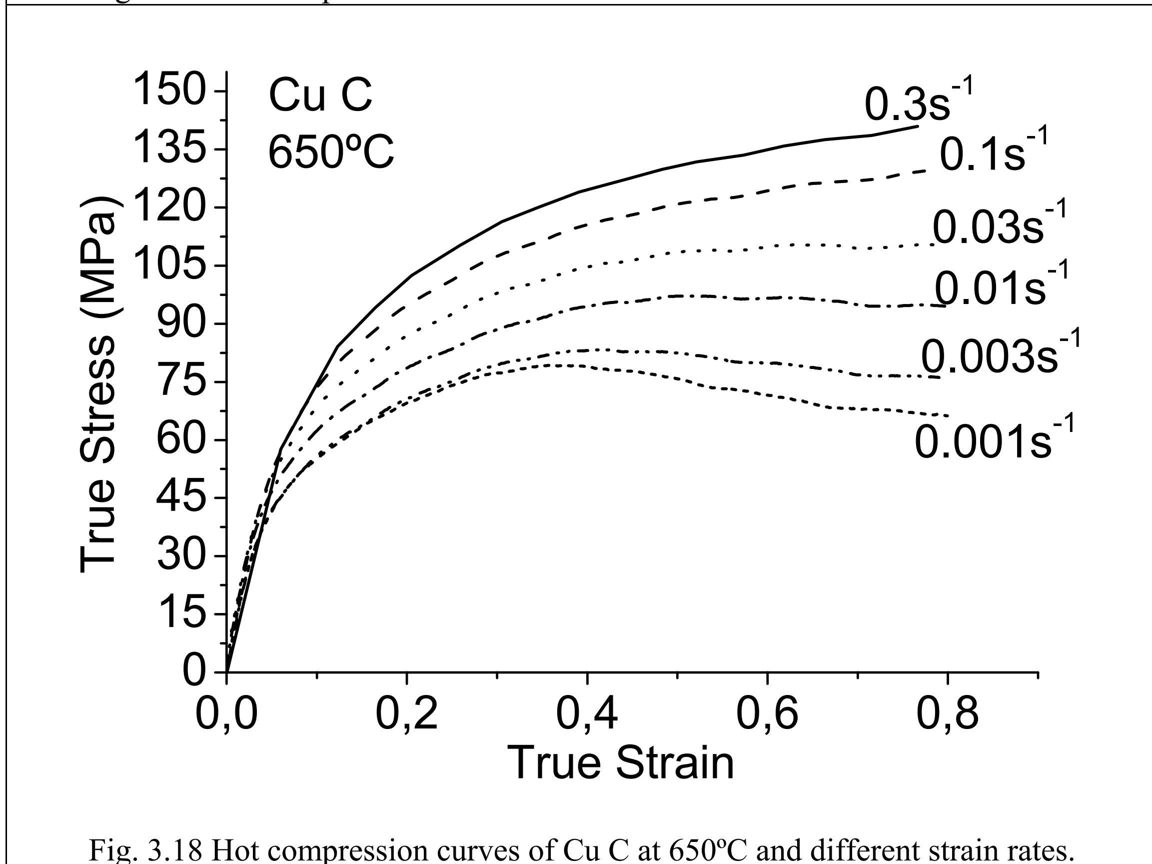

Fig. 3.18 Hot compression curves of Cu C at 650ºC and different strain rates.

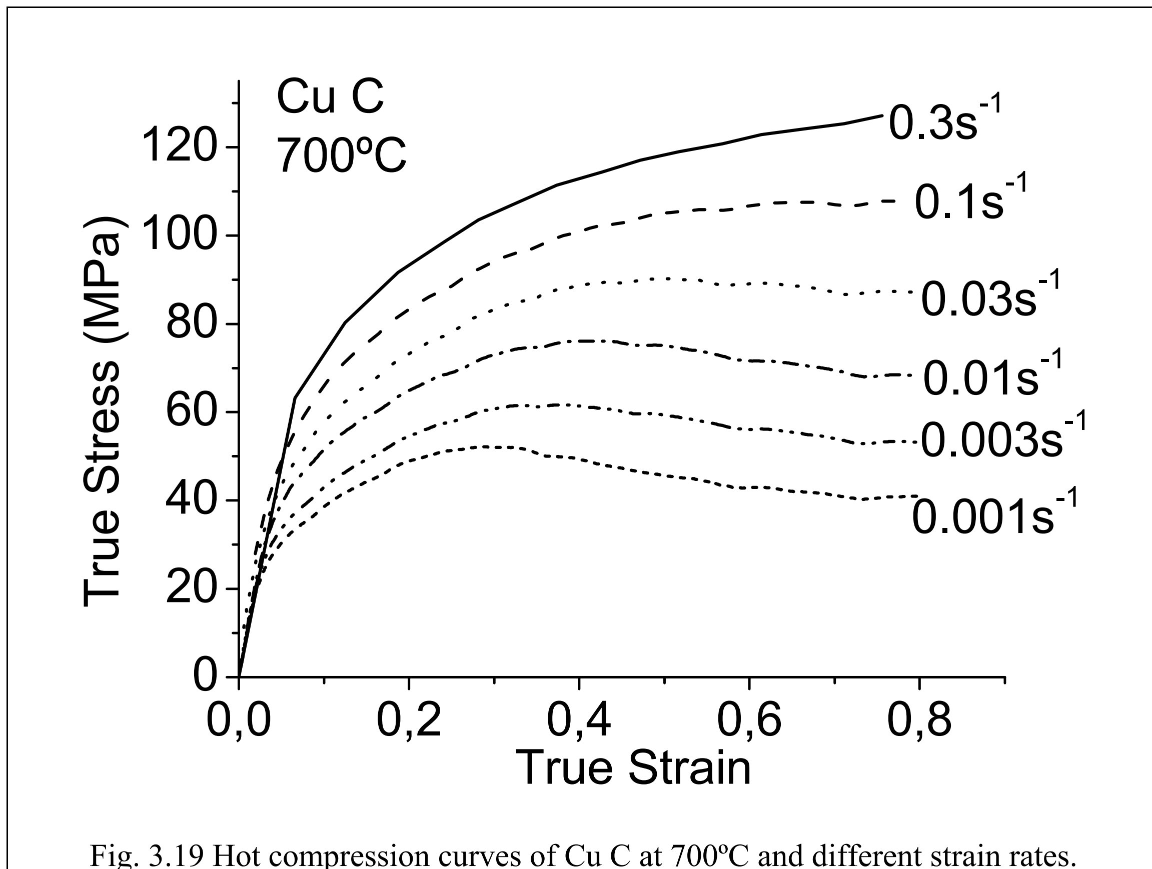

Fig. 3.19 Hot compression curves of Cu C at 700ºC and different strain rates.

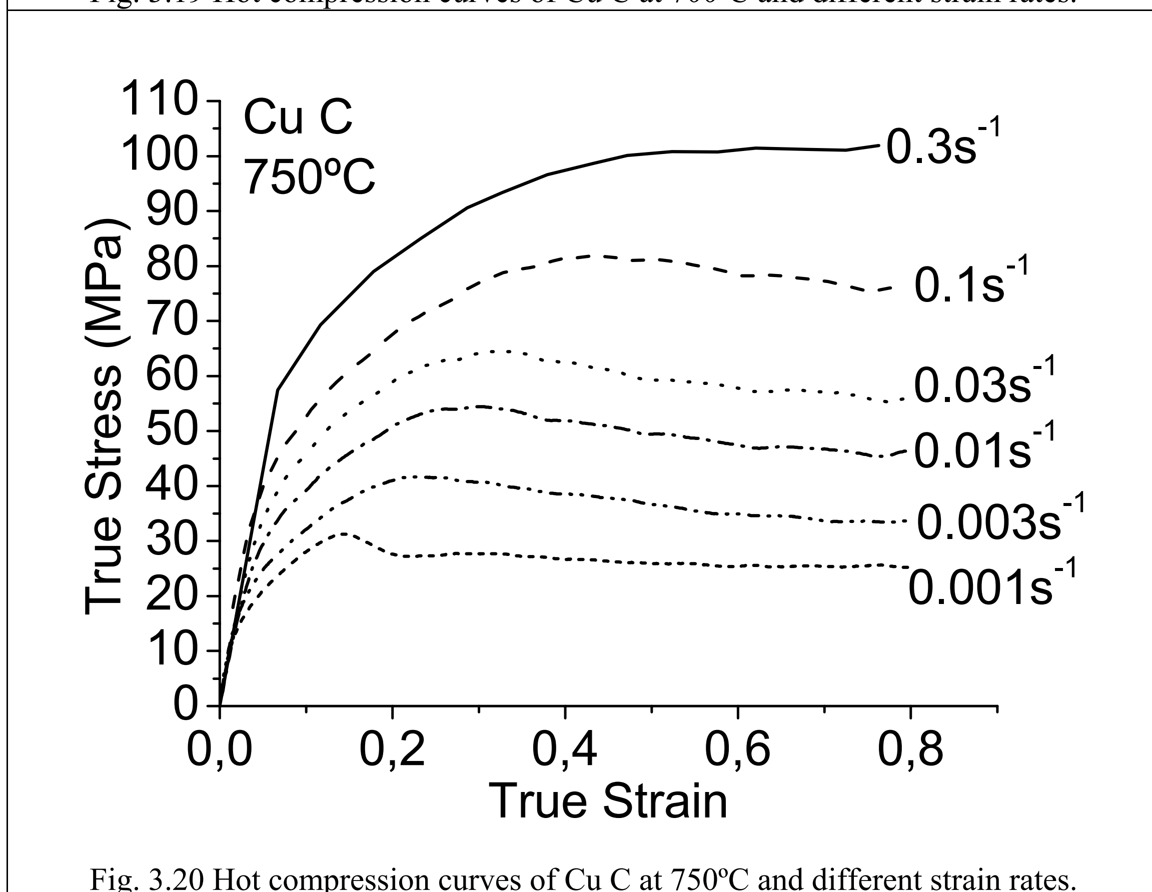

Fig. 3.20 Hot compression curves of Cu C at 750ºC and different strain rates.

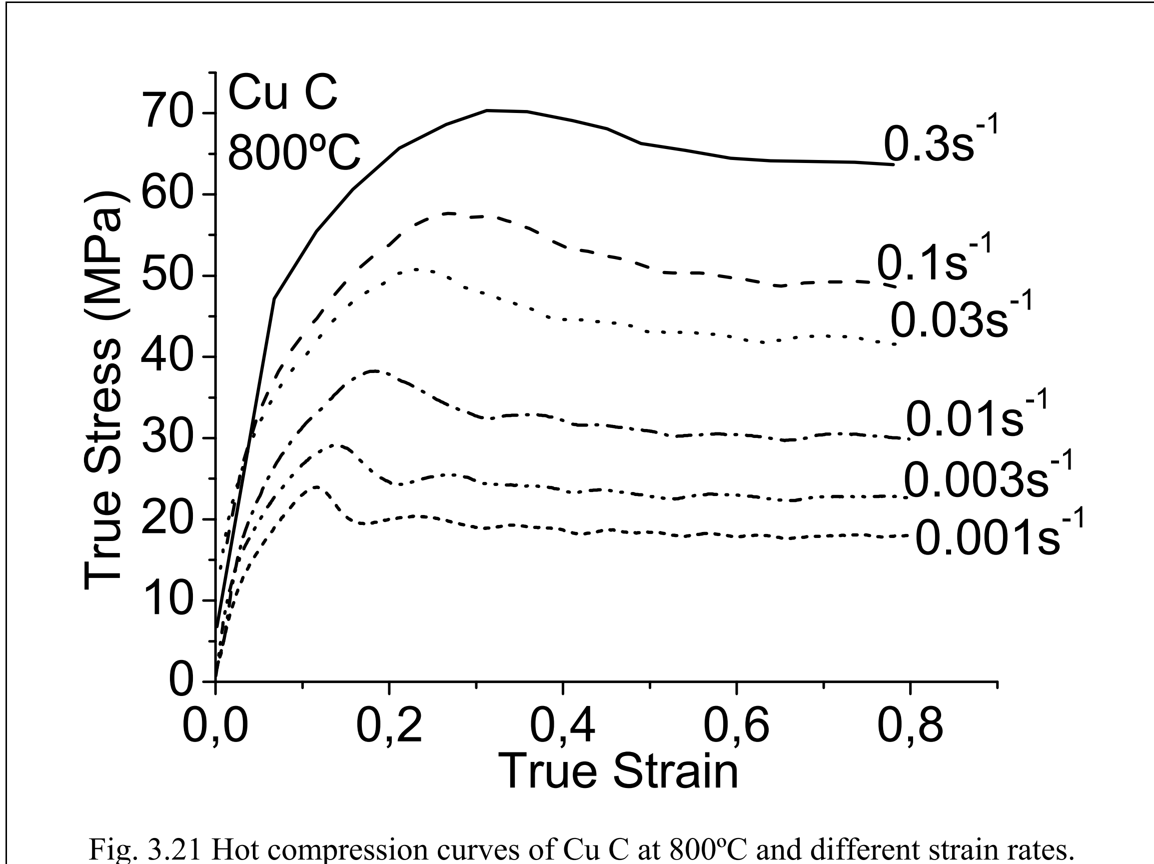

Fig. 3.21 Hot compression curves of Cu C at 800ºC and different strain rates.

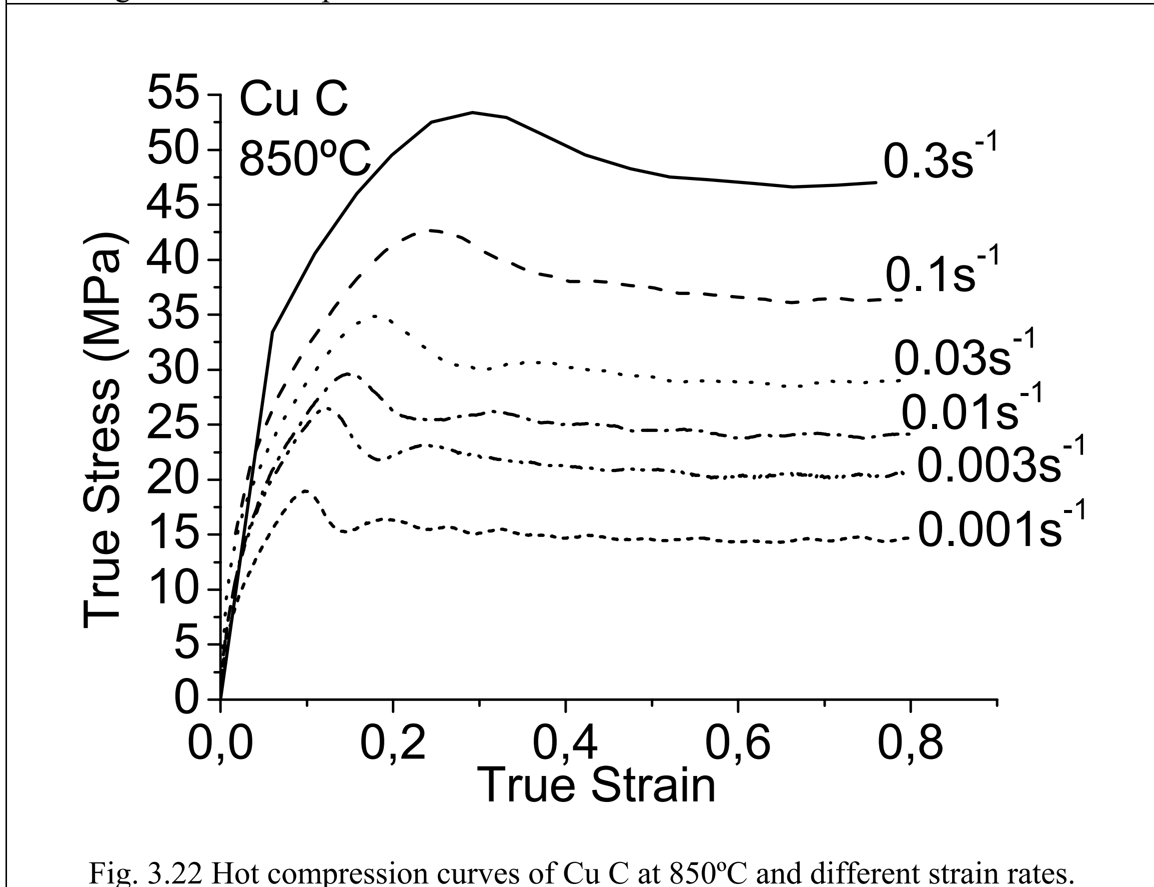

Fig. 3.22 Hot compression curves of Cu C at 850ºC and different strain rates.

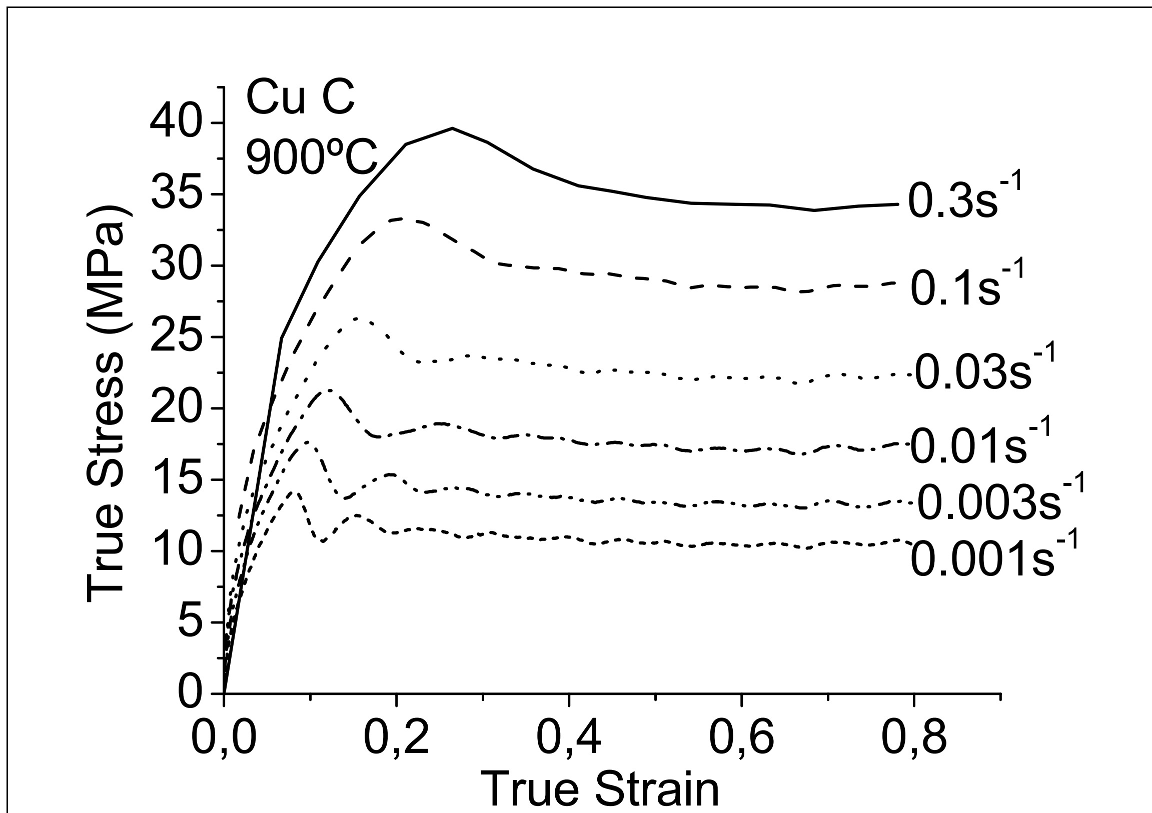

Fig.3.23 Hot compression curves of Cu C at 900ºC and different strain rates.

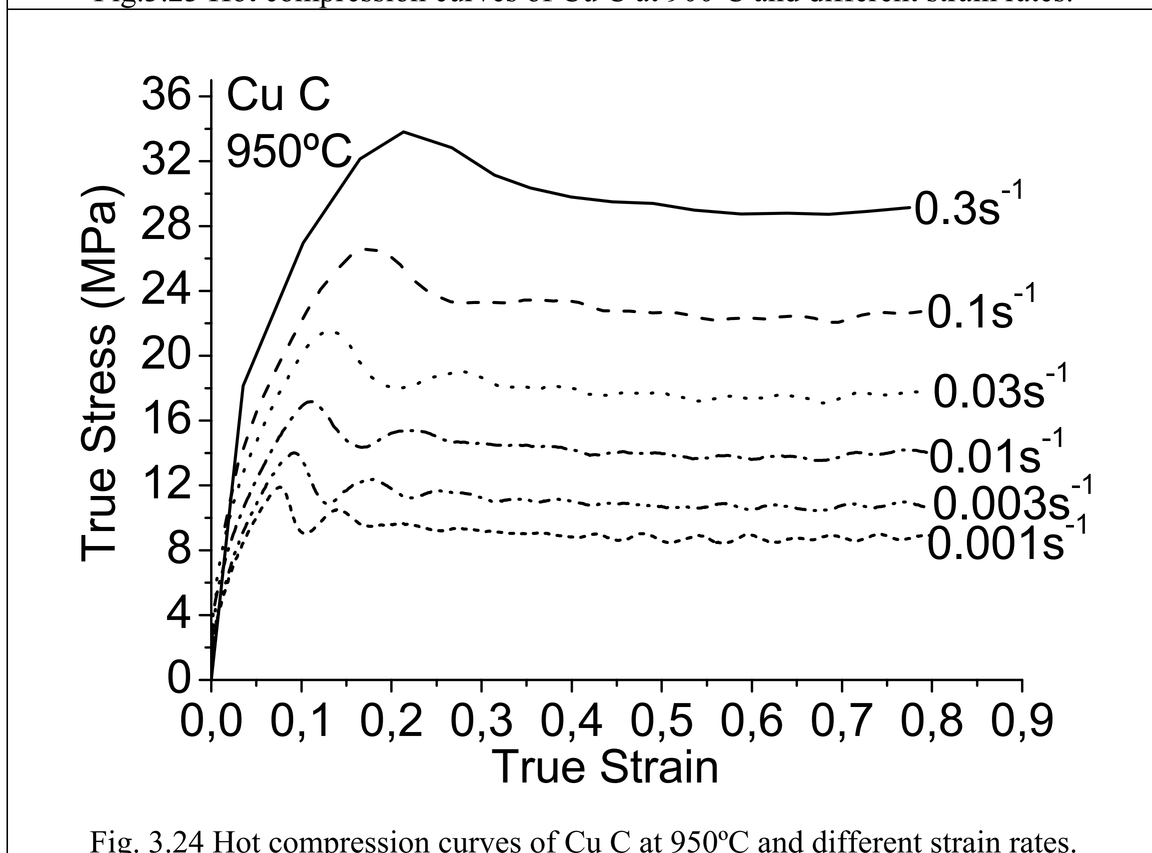

Fig. 3.24 Hot compression curves of Cu C at 950ºC and different strain rates.

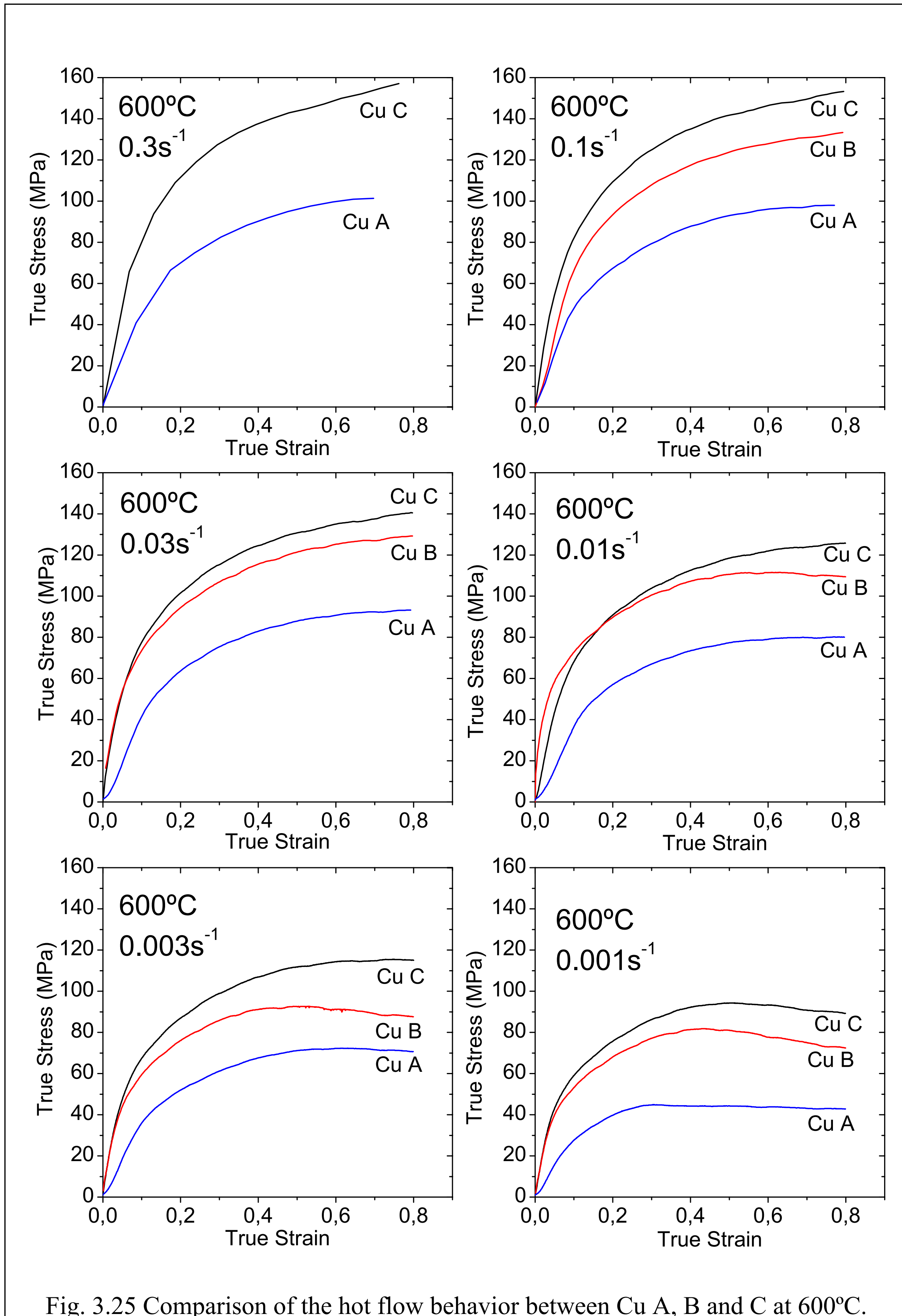

Fig. 3.25 Comparison of the hot flow behavior between Cu A, B and C at 600ºC.

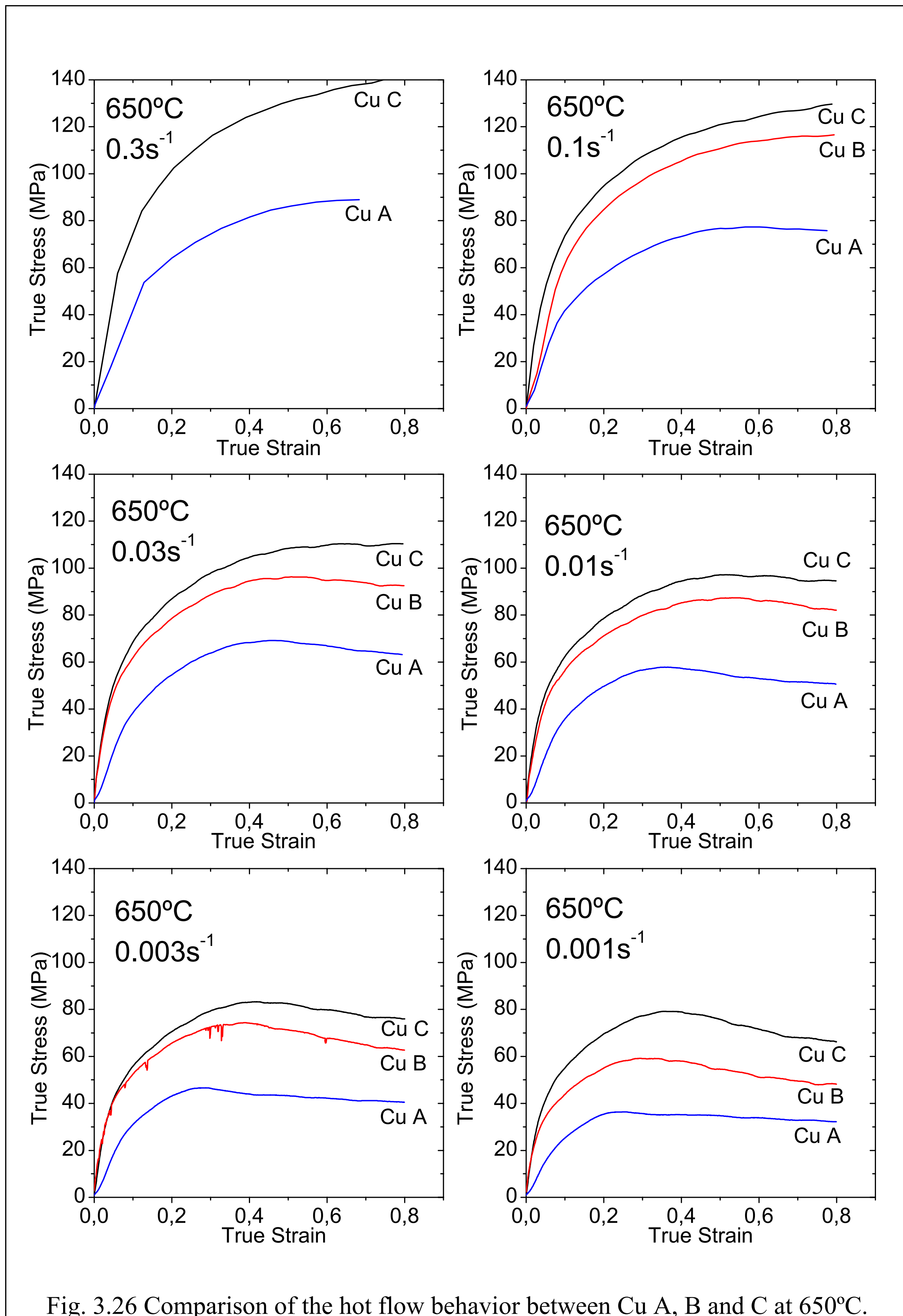

Fig. 3.26 Comparison of the hot flow behavior between Cu A, B and C at 650ºC.

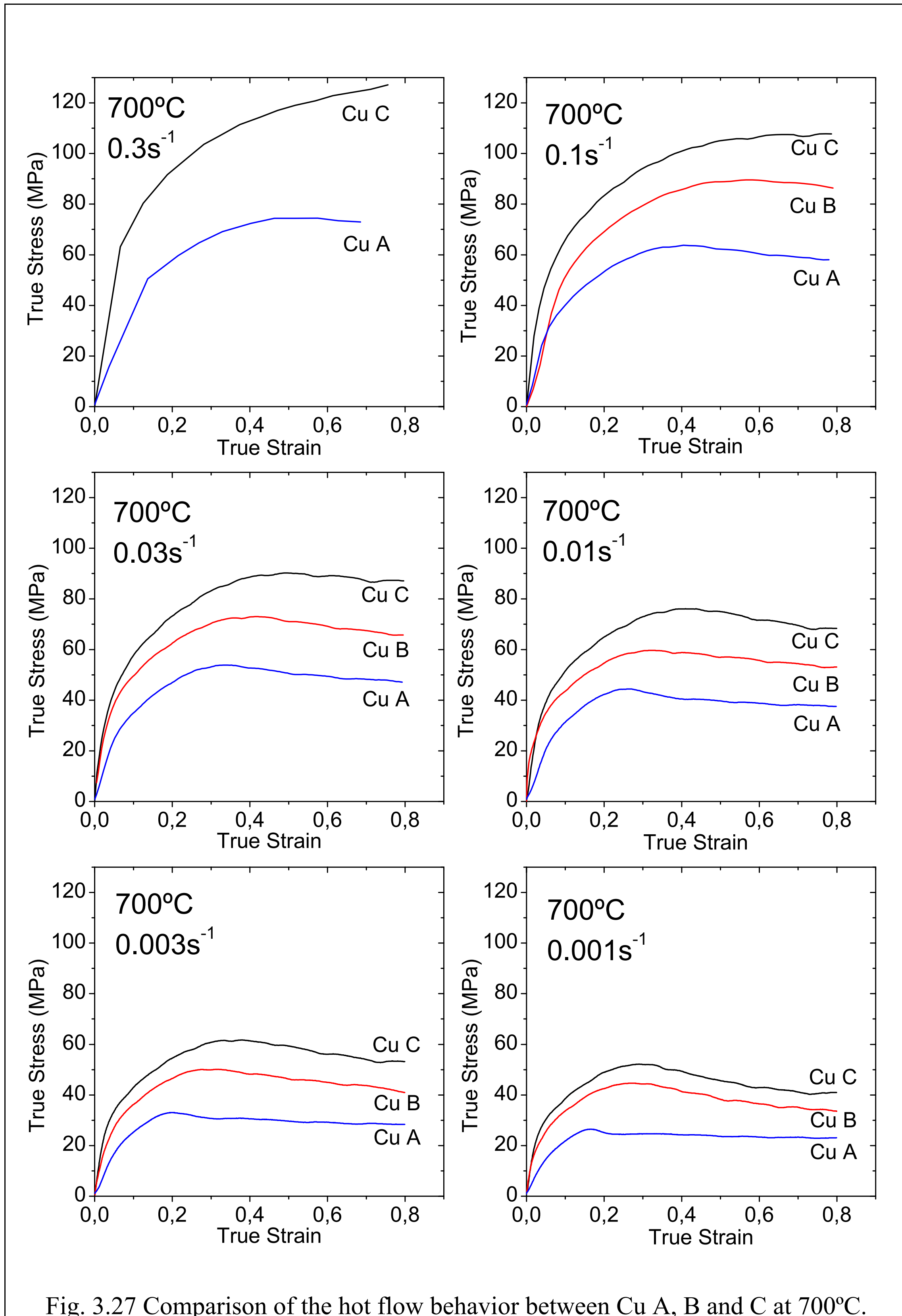

Fig. 3.27 Comparison of the hot flow behavior between Cu A, B and C at 700ºC.

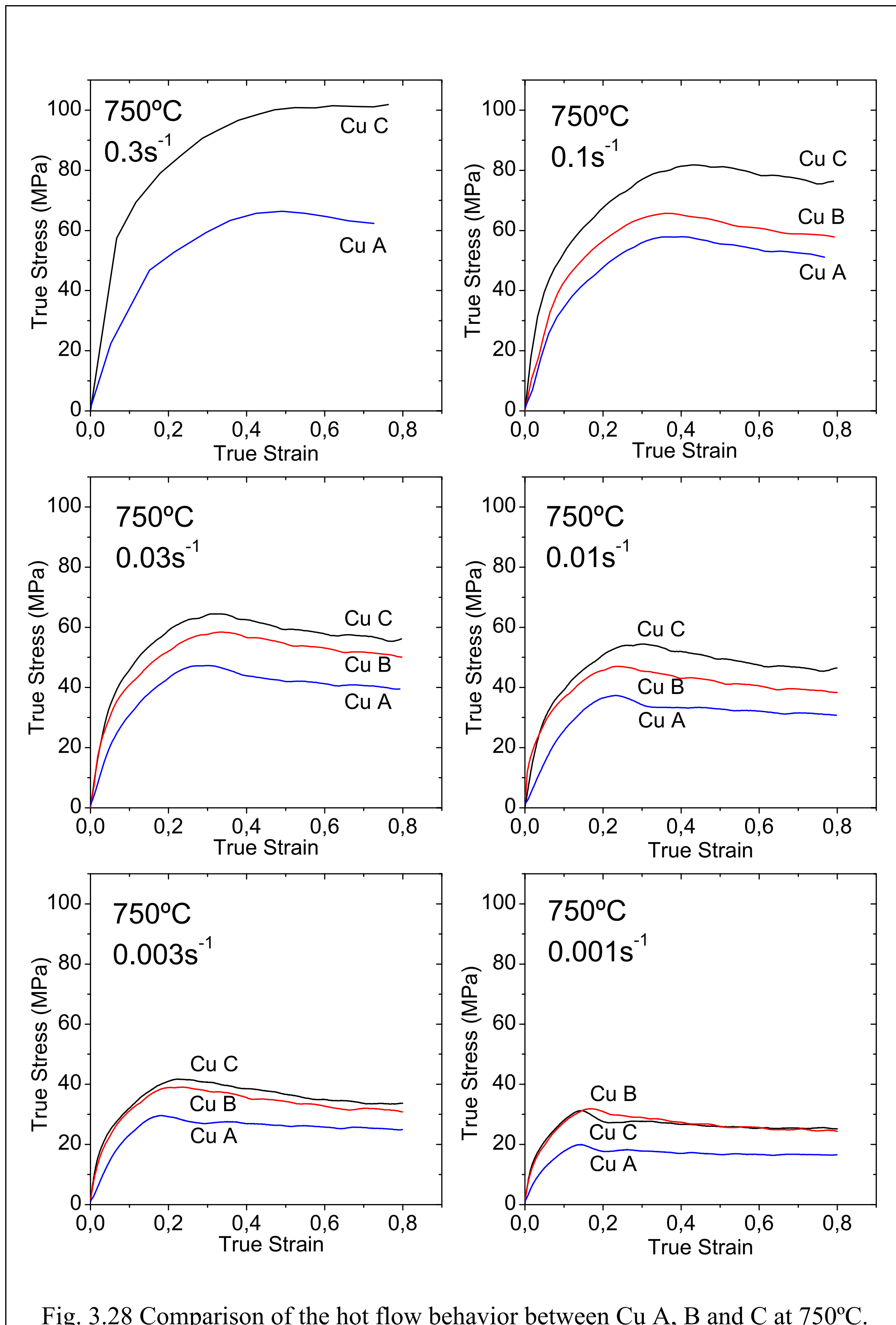

Fig. 3.28 Comparison of the hot flow behavior between Cu A, B and C at 750ºC.

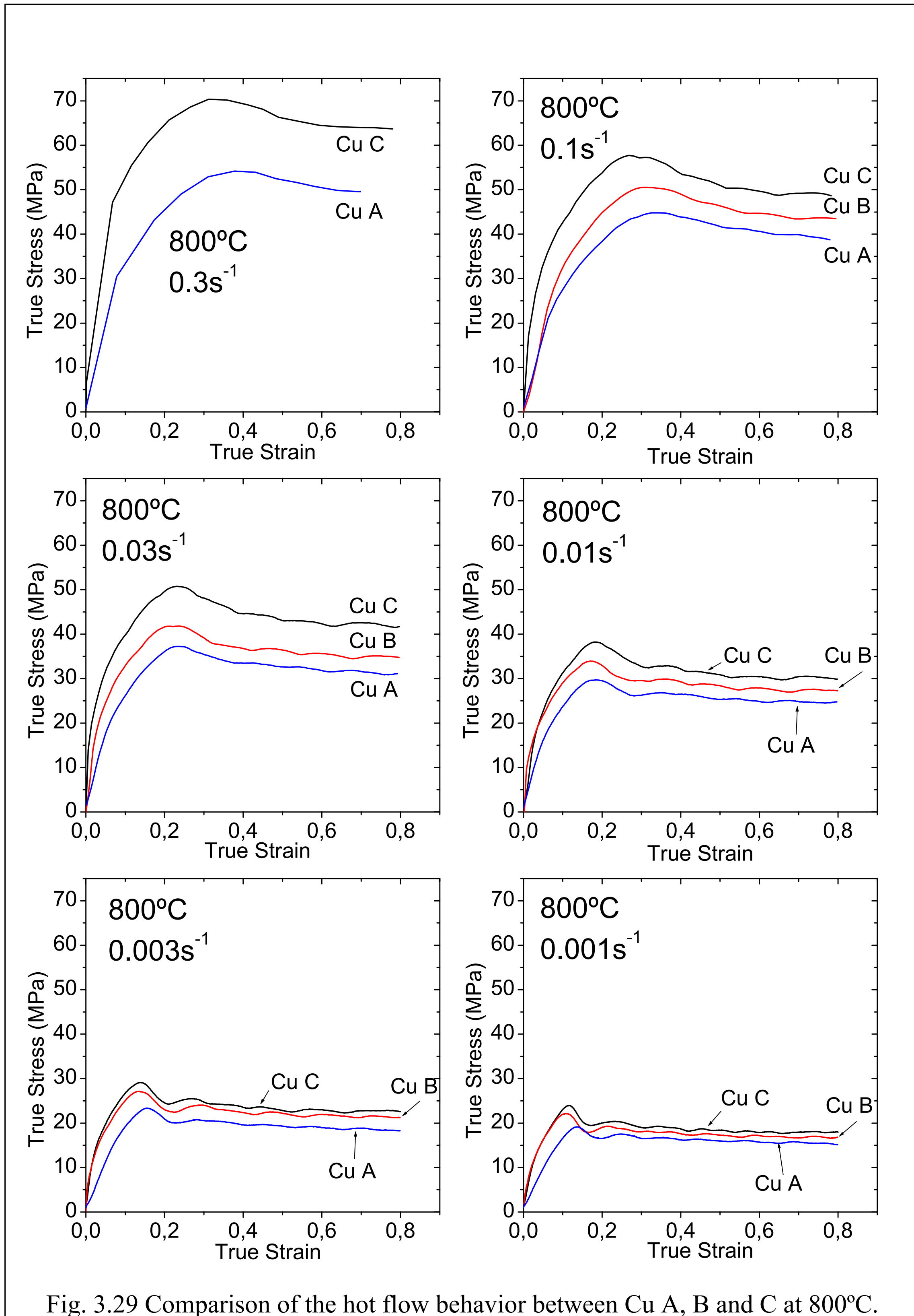

Fig. 3.29 Comparison of the hot flow behavior between Cu A, B and C at 800ºC.

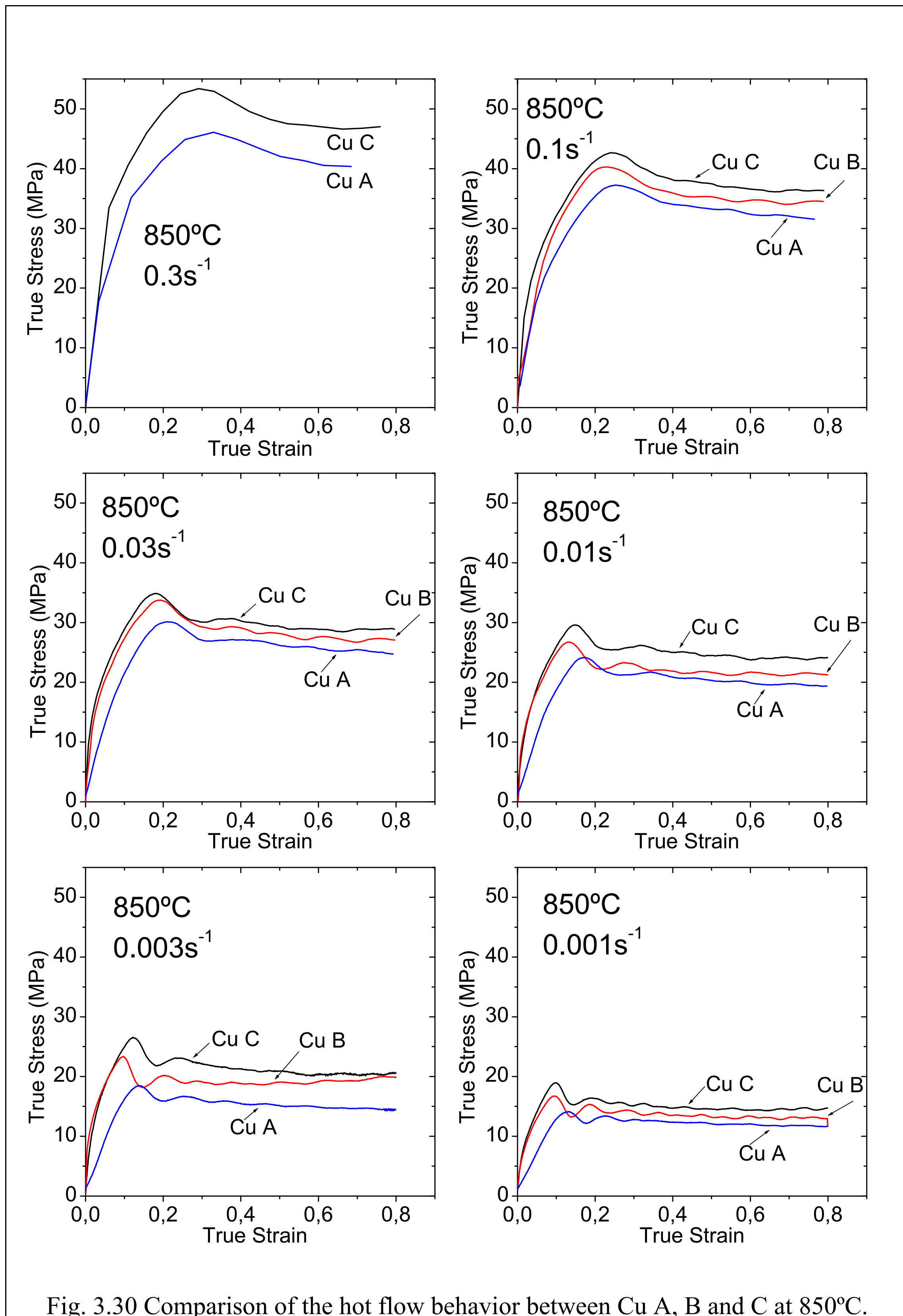

Fig. 3.30 Comparison of the hot flow behavior between Cu A, B and C at 850ºC.

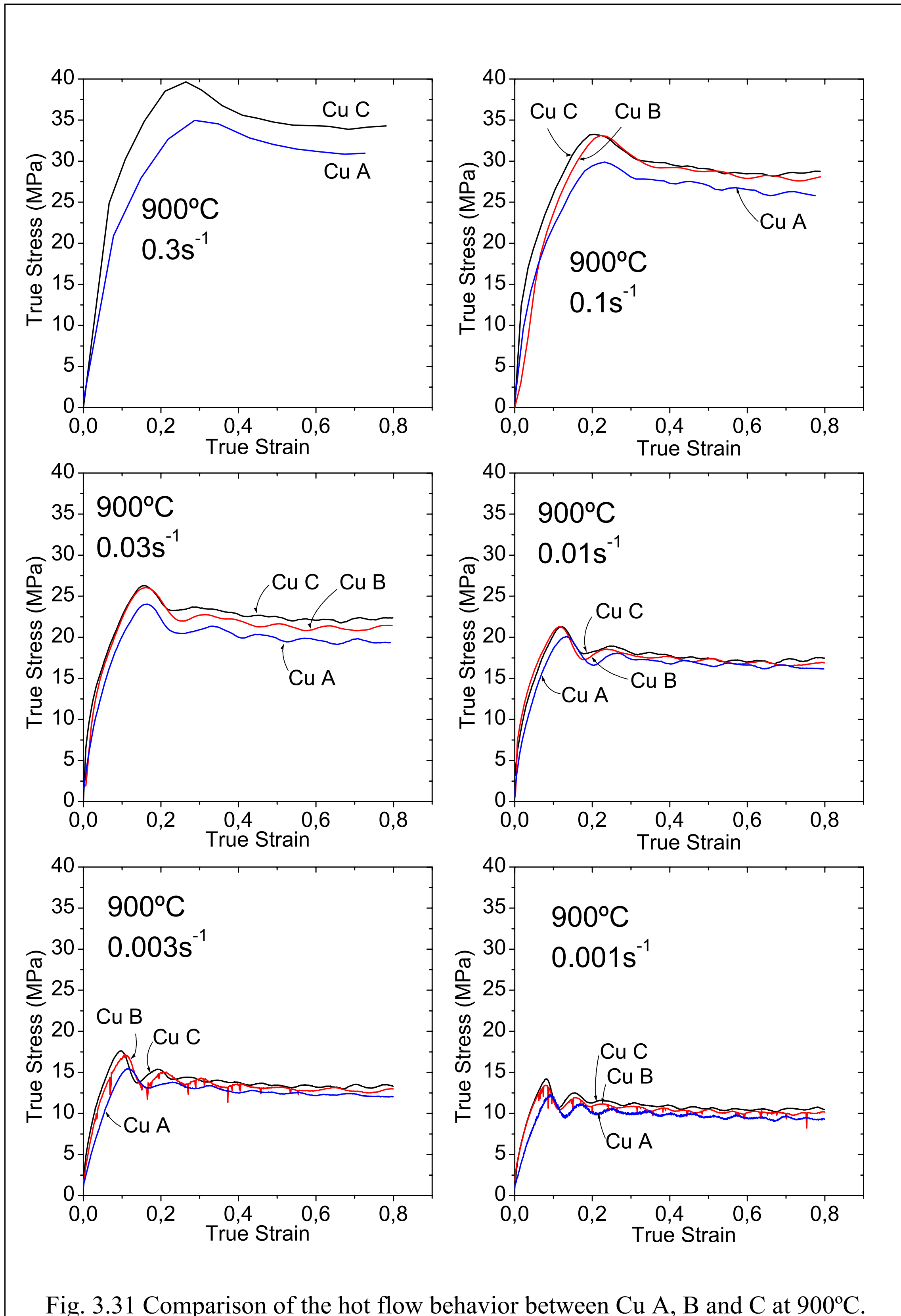

Fig. 3.31 Comparison of the hot flow behavior between Cu A, B and C at 900ºC.

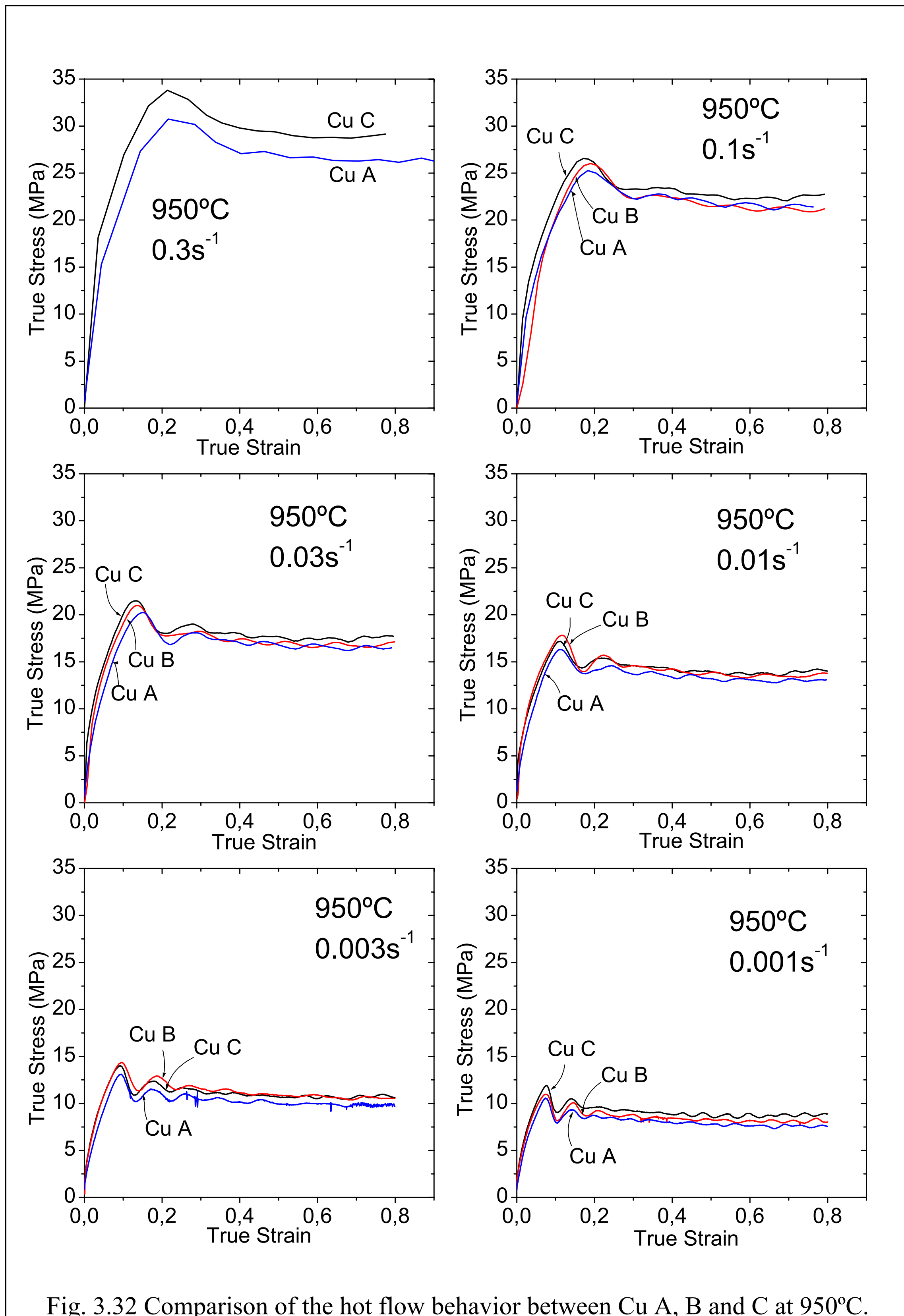

Fig. 3.32 Comparison of the hot flow behavior between Cu A, B and C at 950ºC.

3.2 Dynamically Recrystallized Microstructure

The final microstructure after 0.8 of strain was refined for the three coppers despite some were subjected to multiple peak DRX. The micrograph on fig. 3.33 shows the initial microstructure of Cu A as would be before a hot compression test. On fig. 3.34 a macrograph shows part of the axial section of the cylindrical test piece before compression. As explained the initial grain size of Cu A was 637µm. The images on fig. 3.35 through fig. 3.42 show the final microstructure after hot compressing from 600ºC to 950ºC at different strain rates. The latter images also demonstrate the effectiveness of the polishing procedure employed, which produced few noticeable scratches. Color micrographs were possible due to the use of polarized light in the microscope. The micrographs at lower temperatures and higher strain rates show incomplete DRX even though the onset of DRX from the hot flow curve was not evident (a peak stress). The dynamically recrystallized grain size was smaller as the strain rate was faster. If for example the micrographs at 850ºC on fig. 3.40 are observed one notices that the microstructure is finest for $0.3s^{-1}$ and is coarsest for $0.001s^{-1}$. For the conditions under which complete DRX took place a coarser microstructure was the typical trend as the strain rate was slower.

Fig. 3.33 Microstructure of Cu A after annealing, but before the hot compression tests.

Fig. 3.34 A macrograph of Cu A before compression same as the previous figure. The arrow shows the axial direction of the compression tests. The entire scale measures 0.5mm.

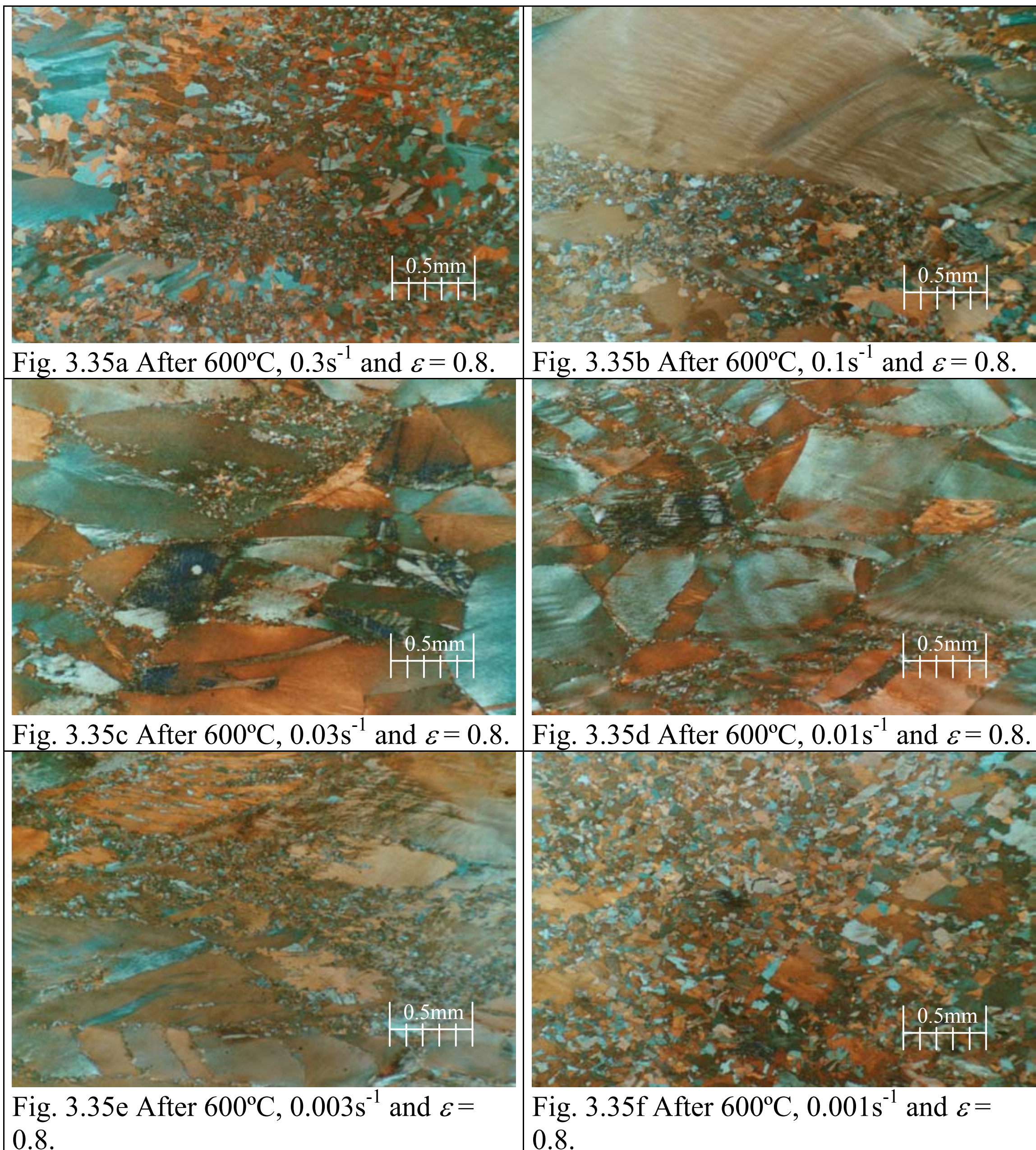

Fig. 3.35a After 600ºC, $0.3s^{-1}$ and $\varepsilon = 0.8$.

Fig. 3.35b After 600ºC, $0.1s^{-1}$ and $\varepsilon = 0.8$.

Fig. 3.35c After 600ºC, $0.03s^{-1}$ and $\varepsilon = 0.8$.

Fig. 3.35d After 600ºC, $0.01s^{-1}$ and $\varepsilon = 0.8$.

Fig. 3.35e After 600ºC, $0.003s^{-1}$ and $\varepsilon = 0.8$.

Fig. 3.35f After 600ºC, $0.001s^{-1}$ and $\varepsilon = 0.8$.

The dynamically recrystallized grain diameter versus strain rate plots behaved similarly for the three coppers under study, particularly at the lower temperatures tested. As expected when the test temperature was increased a larger dynamically recrystallized grain size was produced. The plots on figures 3.42, 3.43 and 3.44 show the dynamically recrystallized grain diameter versus strain rate for Cu A, Cu B and Cu C respectively. As explained graphically, the grain size diminished as the strain rate was faster. Despite statistical and experimental error on figures 3.42, 3.43 and 3.44 the temperature lines almost never cross. This diminishing and never crossing behavior of the temperature lines gives thought to an existing asymptotic grain size at each temperature. The latter plots allow comparing the dynamically recrystallized grain diameter between the test temperatures of a single copper, but are of little help when comparing the three coppers.

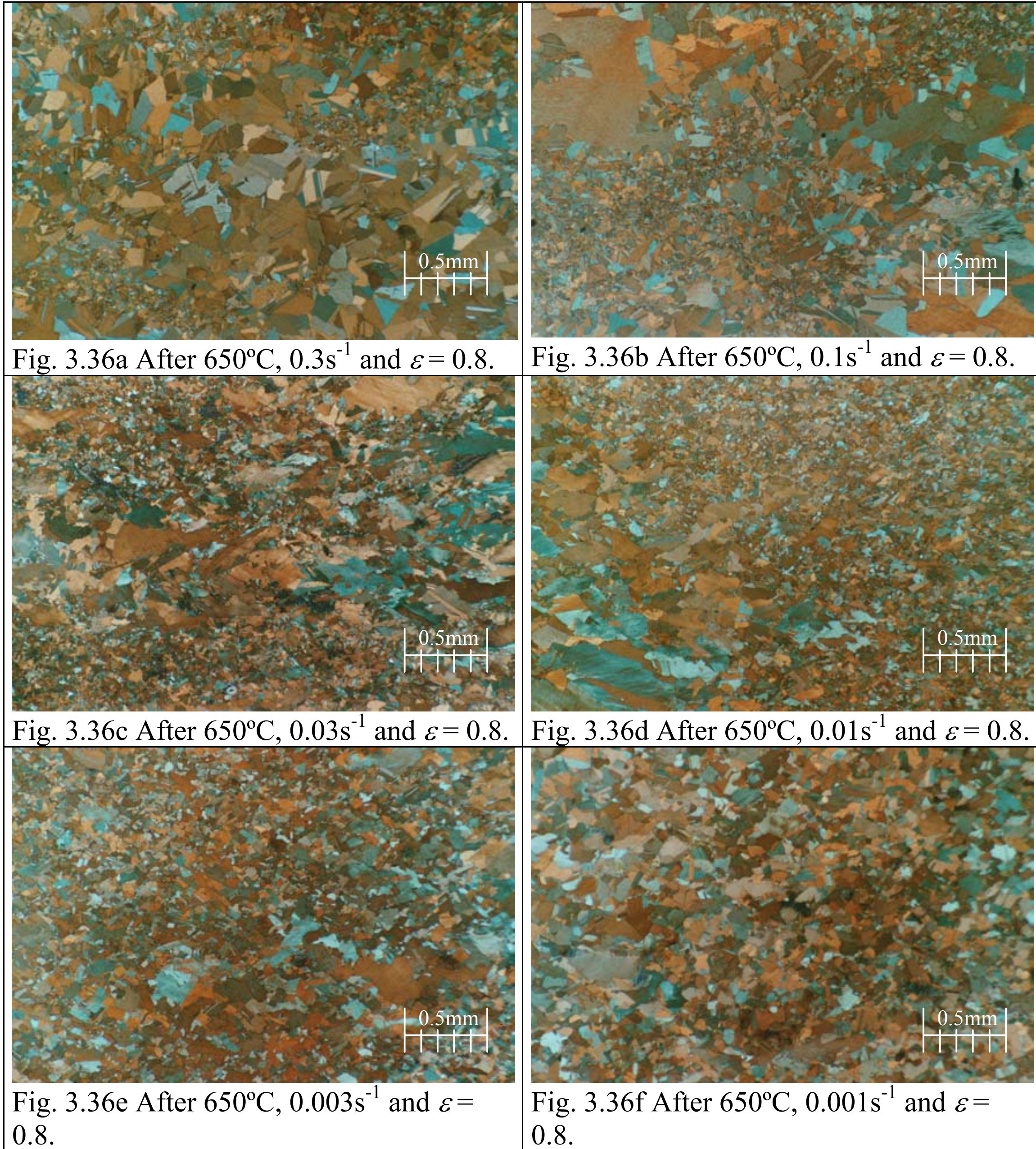

Fig. 3.36a After 650ºC, 0.3s^{-1} and $\varepsilon = 0.8$.

Fig. 3.36b After 650ºC, 0.1s^{-1} and $\varepsilon = 0.8$.

Fig. 3.36c After 650ºC, 0.03s^{-1} and $\varepsilon = 0.8$.

Fig. 3.36d After 650ºC, 0.01s^{-1} and $\varepsilon = 0.8$.

Fig. 3.36e After 650ºC, 0.003s^{-1} and $\varepsilon = 0.8$.

Fig. 3.36f After 650ºC, 0.001s^{-1} and $\varepsilon = 0.8$.

The plots at different temperatures seen on fig 3.46 allowed comparing the dynamically recrystallized grain size between the three coppers. At 850ºC and below the produced grain size is similar in the three coppers, but at the higher temperatures of 900ºC and 950ºC the differences are noticeable despite some scatter. In fig. 3.46 the scale of the 950ºC plot is more than double the scale of the other plots, a detail that must be bared in mind when acknowledging that at high temperatures fire refined coppers can produce different dynamically recrystallized grain sizes. At temperatures above 850ºC one can see that in global terms Cu A (represented by a triangle in fig. 3.46) has the largest grain size followed by Cu C (represented by a square). The finest grain sizes were observed in Cu B (represented by a circle). This order correlates well with the amount of the most significant solute elements, i.e. Pb, Ni and Ag, but not with the oxygen content. This feature can be explained bearing in mind that the oxygen-copper particles should be dissolved at 900ºC and 950ºC. At these high temperatures solute

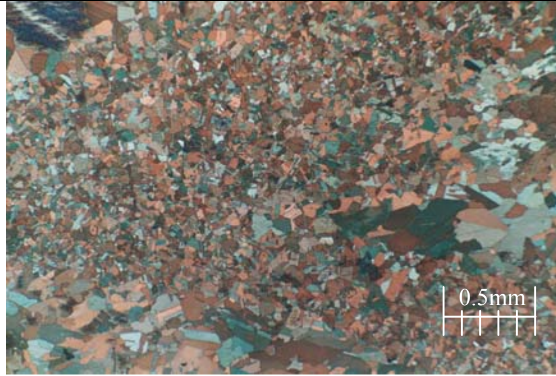

Fig. 3.37a After 700ºC, $0.1s^{-1}$ and $\varepsilon = 0.8$.

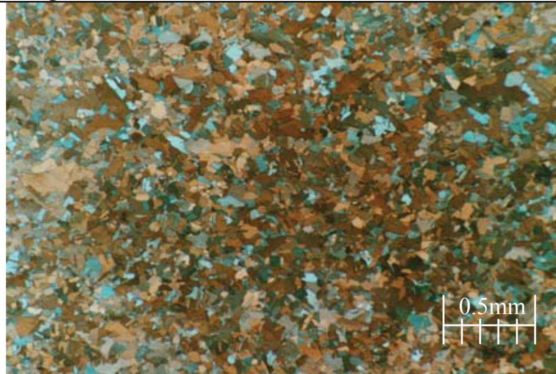

Fig. 3.37b After 700ºC, $0.01s^{-1}$ and $\varepsilon = 0.8$.

Fig. 3.37c After 700ºC, $0.001s^{-1}$ and $\varepsilon = 0.8$.

drag of Ni and Ag or second phase particles of Pb are probably influencing nucleation of new grains. At higher temperatures nucleation has been described by the formation of annealing twins, which gradually lose coherency and form a new grain [6, 7]. The residual amount at higher temperatures of Ni, Ag and Pb indirectly affect the grain growth of the three coppers. On the other hand at lower temperatures the combined effect of oxygen-copper particles (concurrently precipitating), the Pb particles and the solute drag are promoting similar grain sizes in the three coppers. The assumption is that at lower temperatures the size and volume fraction of Pb particles remain constant with temperature, also that the weak solute drag effect on Ni and Ag continues, then the similar grain sizes in the three coppers can be mainly attributed to the increasing precipitation of oxygen-copper particles.

<table>
<tr><td>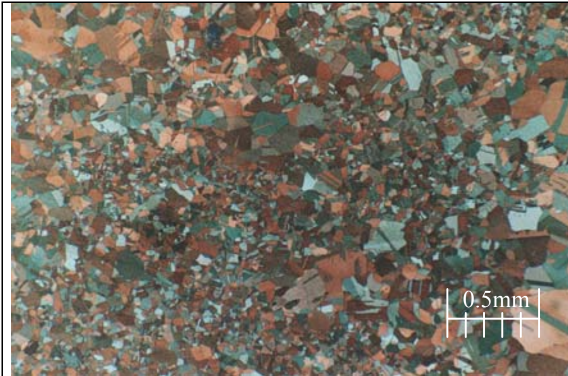

Fig. 3.38a After 750ºC, 0.3s^{-1} and $\varepsilon = 0.8$.</td><td>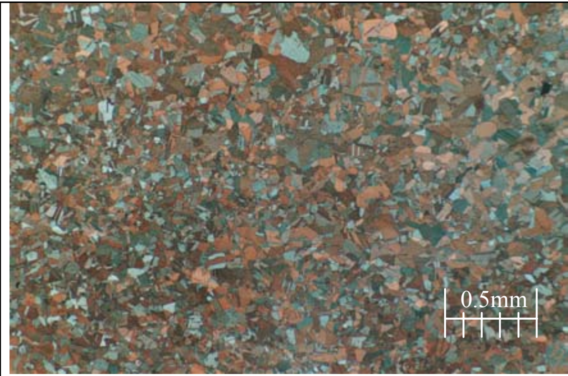

Fig. 3.38b After 750ºC, 0.1s^{-1} and $\varepsilon = 0.8$.</td></tr>
<tr><td>

Fig. 3.38c After 750ºC, 0.03s^{-1} and $\varepsilon = 0.8$.</td><td>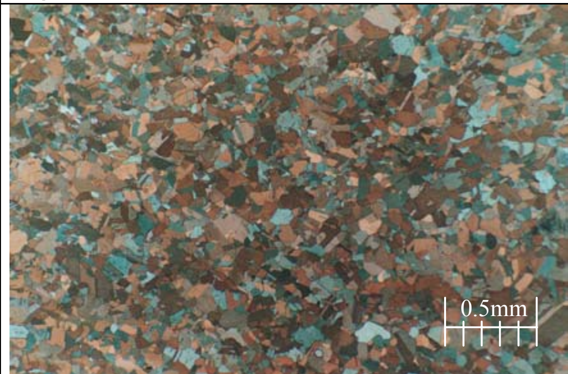

Fig. 3.38d After 750ºC, 0.01s^{-1} and $\varepsilon = 0.8$.</td></tr>
<tr><td>

Fig. 3.38e After 750ºC, 0.003s^{-1} and $\varepsilon =$ 0.8.</td><td>

Fig. 3.38f After 750ºC, 0.001s^{-1} and $\varepsilon =$ 0.8.</td></tr>
</table>

<table>
<tr><td>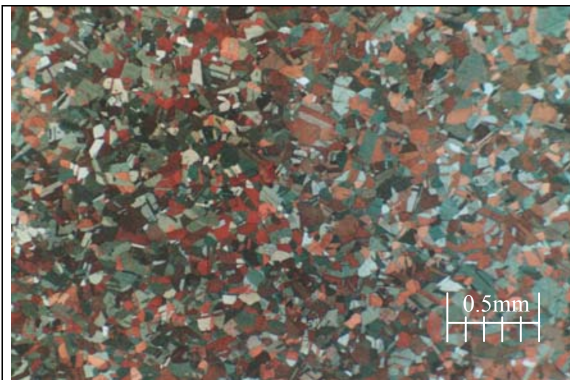

Fig. 3.39a After 800ºC, 0.1s^{-1} and $\varepsilon = 0.8$.</td><td>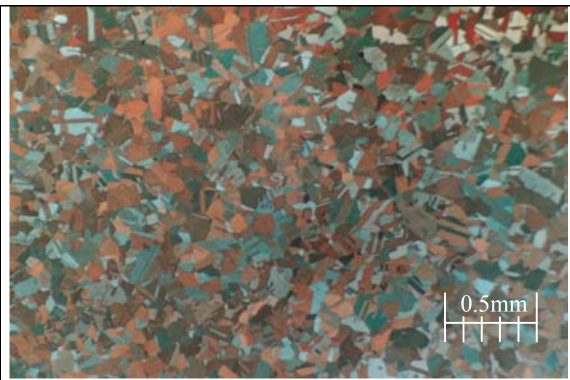

Fig. 3.39b After 800ºC, 0.03s^{-1} and $\varepsilon = 0.8$.</td></tr>
<tr><td>

Fig. 3.39c After 800ºC, 0.01s^{-1} and $\varepsilon = 0.8$.</td><td>

Fig. 3.39d After 800ºC, 0.001s^{-1} and $\varepsilon = 0.8$.</td></tr>
</table>

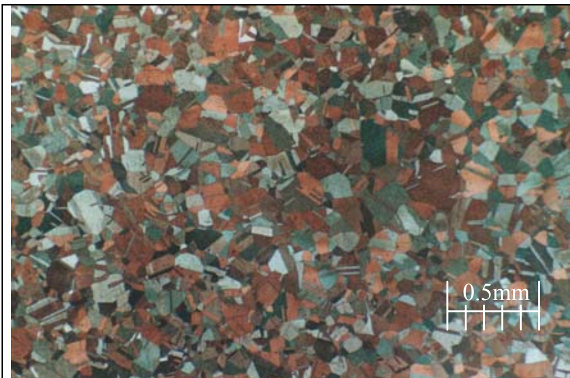 Fig. 3.40a After 850ºC, $0.3s^{-1}$ and $\varepsilon = 0.8$.	Fig. 3.40b After 850ºC, $0.1s^{-1}$ and $\varepsilon = 0.8$.
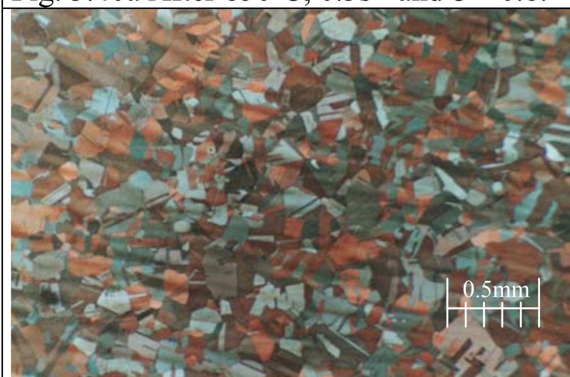 Fig. 3.40c After 850ºC, $0.03s^{-1}$ and $\varepsilon = 0.8$.	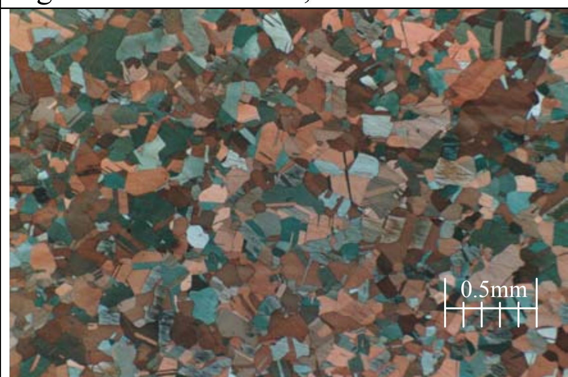 Fig. 3.40d After 850ºC, $0.01s^{-1}$ and $\varepsilon = 0.8$.
Fig. 3.40e After 850ºC, $0.003s^{-1}$ and $\varepsilon = 0.8$.	Fig. 3.40f After 850ºC, $0.001s^{-1}$ and $\varepsilon = 0.8$.

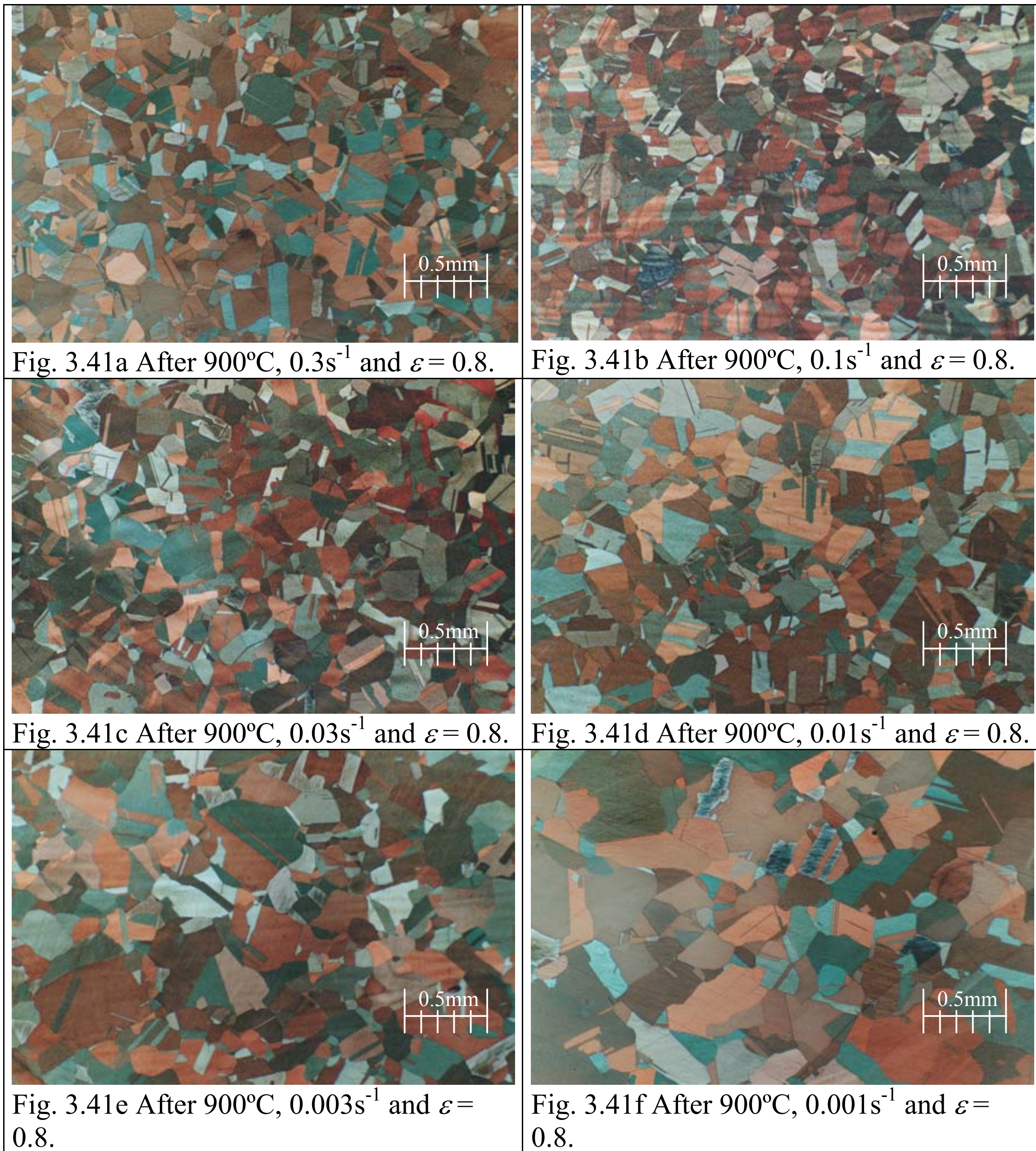

Fig. 3.41a After 900ºC, 0.3s^{-1} and $\varepsilon = 0.8$.

Fig. 3.41b After 900ºC, 0.1s^{-1} and $\varepsilon = 0.8$.

Fig. 3.41c After 900ºC, 0.03s^{-1} and $\varepsilon = 0.8$.

Fig. 3.41d After 900ºC, 0.01s^{-1} and $\varepsilon = 0.8$.

Fig. 3.41e After 900ºC, 0.003s^{-1} and $\varepsilon = 0.8$.

Fig. 3.41f After 900ºC, 0.001s^{-1} and $\varepsilon = 0.8$.

<table>
<tr><td>

Fig. 3.42a After 950ºC, 0.3s^{-1} and $\varepsilon = 0.8$.</td><td>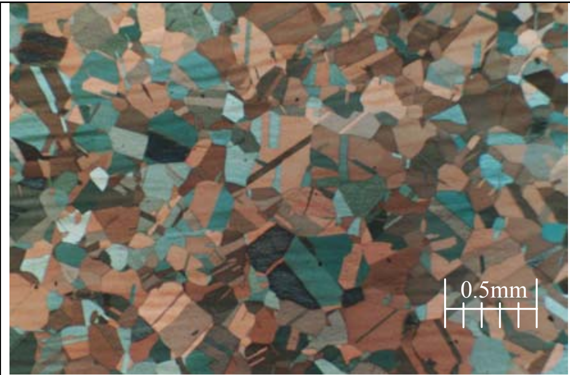

Fig. 3.42b After 950ºC, 0.1s^{-1} and $\varepsilon = 0.8$.</td></tr>
<tr><td>

Fig. 3.42c After 950ºC, 0.03s^{-1} and $\varepsilon = 0.8$.</td><td>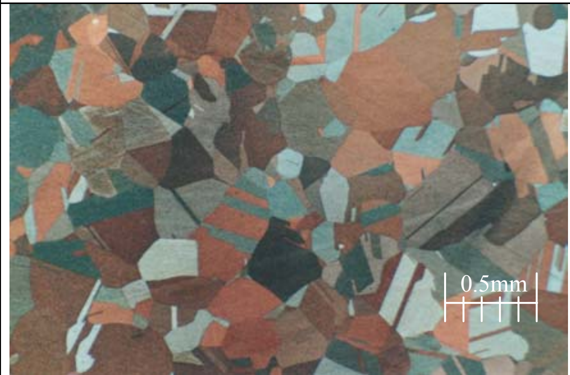

Fig. 3.42d After 950ºC, 0.01s^{-1} and $\varepsilon = 0.8$.</td></tr>
<tr><td>

Fig. 3.42e After 950ºC, 0.003s^{-1} and $\varepsilon = 0.8$.</td><td>

Fig. 3.42f After 950ºC, 0.001s^{-1} and $\varepsilon = 0.8$.</td></tr>
</table>

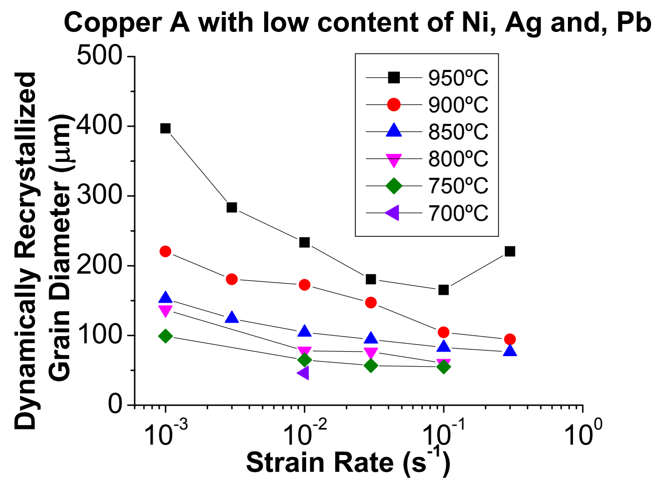

Fig. 3.43 The dynamically recrystallized grain diameters versus strain rate of Cu A. Twin boundaries were not included. Only micrographs with complete DRX were accounted.

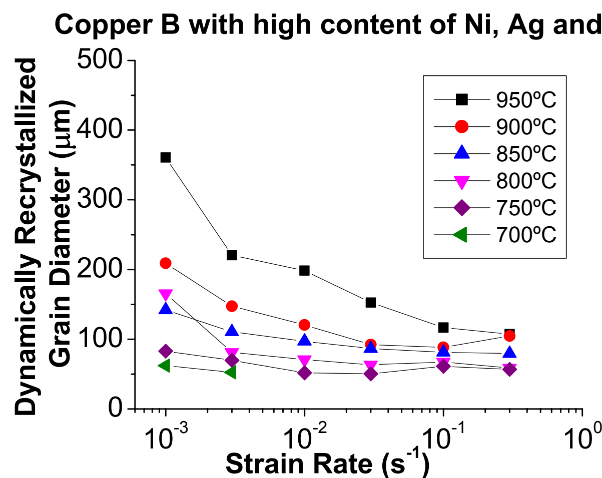

Fig. 3.44 The dynamically recrystallized grain diameters versus strain rate of Cu B. Twin boundaries were not included. Only micrographs with complete DRX were accounted.

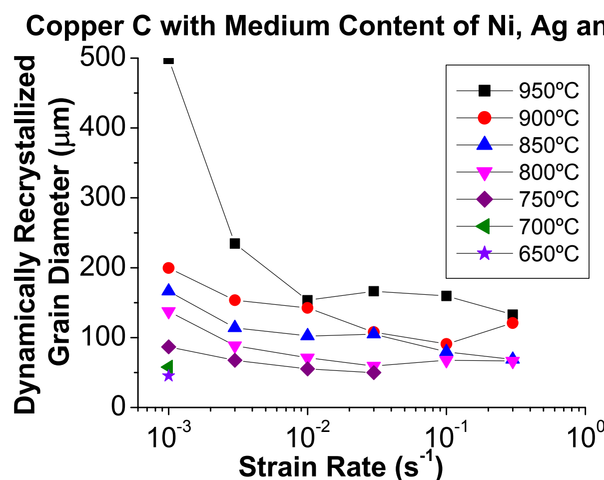

Fig. 3.45 The dynamically recrystallized grain diameters versus strain rate of Cu C. Twin boundaries were not included. Only micrographs with complete DRX were accounted.

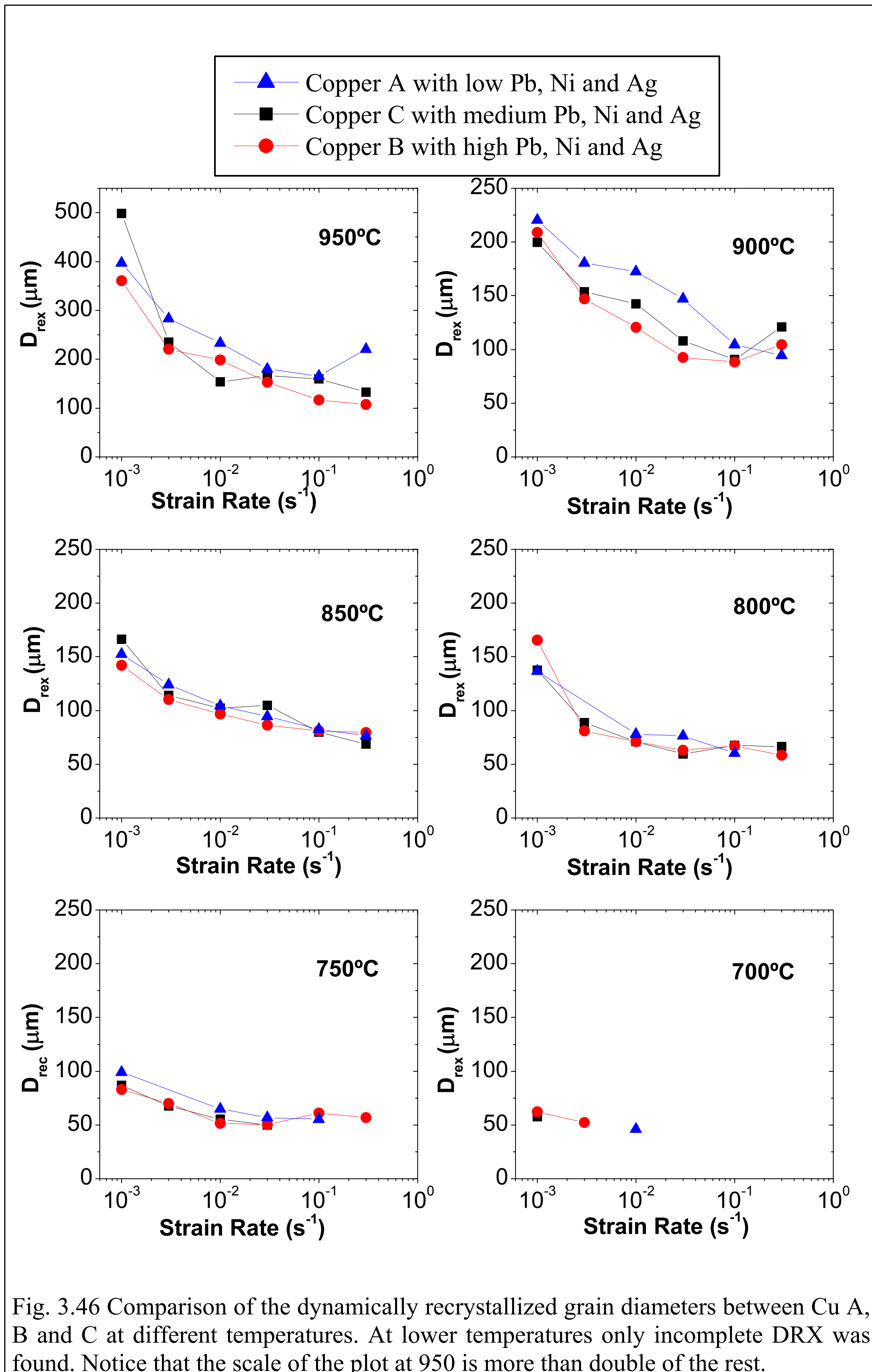

Fig. 3.46 Comparison of the dynamically recrystallized grain diameters between Cu A, B and C at different temperatures. At lower temperatures only incomplete DRX was found. Notice that the scale of the plot at 950 is more than double of the rest.

3.3 Grain Growth Studies

The grain growth studies of Cu A [8] and Cu C demonstrate the rate of static growth of the as-received material at the temperatures employed on earlier hot compression tests. The static grain growth rate is probably slower than a dynamical growth rate, but a minimum estimate of how fast a grain grows was obtained. Also undoubtedly post dynamical grain growth occurred in the few instants between the hot compression test and the quenching. A grain growth study helps to understand how the latter post dynamical grain growth might have affected the observed grain on the final microstructure. The plot by Rius et al. [8] on fig. 3.47 shows a grain diameter growth versus time inside the oven of Cu A performed at 950ºC, 900ºC, 850ºC and 800ºC. The scale of the study was conveniently separated to appreciate the behavior at lower temperatures thus on fig. 3.48 the plot at 750ºC, 700ºC, 650ºC and 600ºC is presented.

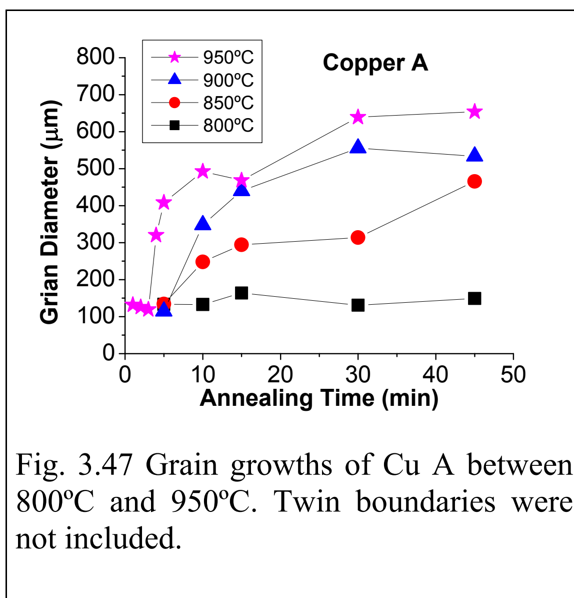

Fig. 3.47 Grain growths of Cu A between 800ºC and 950ºC. Twin boundaries were not included.

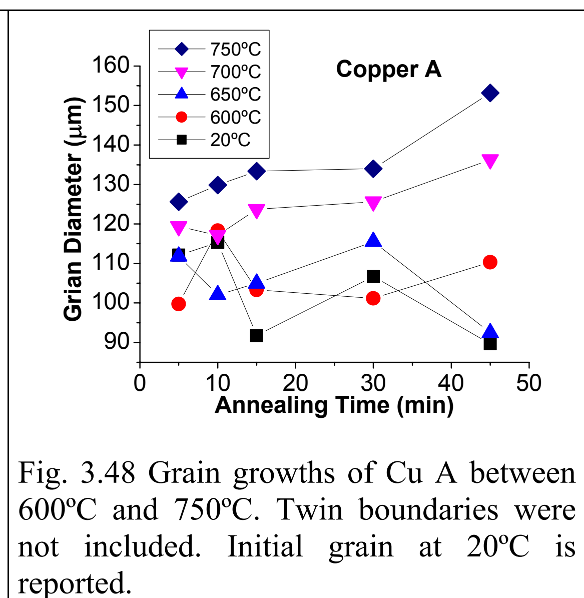

Fig. 3.48 Grain growths of Cu A between 600ºC and 750ºC. Twin boundaries were not included. Initial grain at 20ºC is reported.

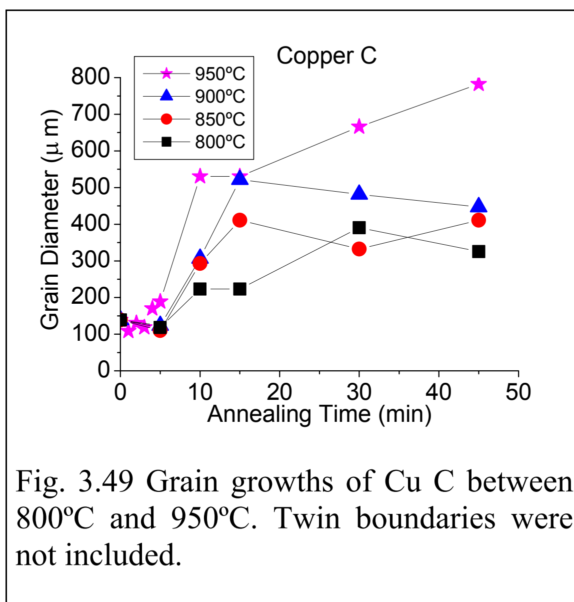

Fig. 3.49 Grain growths of Cu C between 800ºC and 950ºC. Twin boundaries were not included.

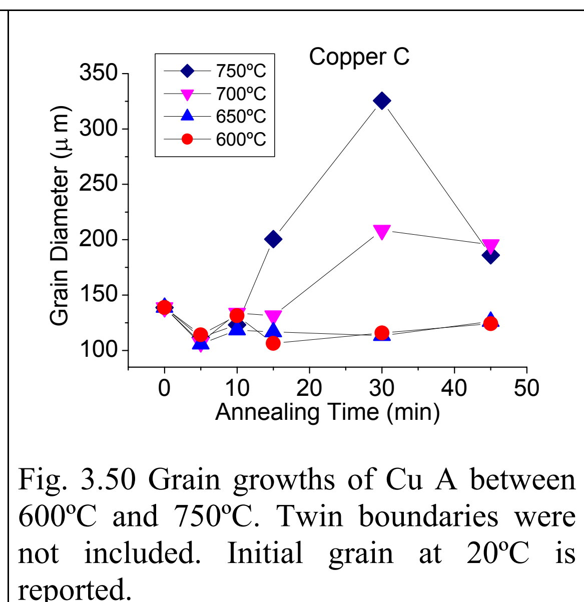

Fig. 3.50 Grain growths of Cu A between 600ºC and 750ºC. Twin boundaries were not included. Initial grain at 20ºC is reported.